Agricultural and Forest Meteorology 342 (2023) 109696

Contents lists available at ScienceDirect

Agricultural and Forest Meteorology

journal homepage: www.elsevier.com/locate/agrformet

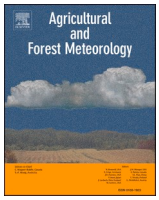

Interannual variability of carbon dioxide (CO_2) and methane (CH_4) fluxes in a rewetted temperate bog

Tin W. Satriawan [a,b,*], Marion Nyberg [a], Sung-Ching Lee [a,c], Andreas Christen [d], T. Andrew Black [e], Mark S. Johnson [f,g], Zoran Nesic [e], Markus Merkens [h], Sara H. Knox [a,i]

[a] Department of Geography, The University of British Columbia, Vancouver, BC, Canada
[b] Department of Geography, National University of Singapore, Singapore
[c] Department Biogeochemical Integration, Max Planck Institute for Biogeochemistry, Jena, Germany
[d] Chair of Environmental Meteorology, Faculty of Environment and Natural Resources, University of Freiburg, Freiburg im Breisgau, Germany
[e] Faculty of Land and Food Systems, The University of British Columbia, Vancouver, BC, Canada
[f] Institute of Resources, Environment and Sustainability, The University of British Columbia, Vancouver, BC, Canada
[g] Department of Earth, Ocean and Atmospheric Sciences, The University of British Columbia, Vancouver, BC, Canada
[h] Parks and Environment, Metro Vancouver Regional District, Burnaby, BC, Canada
[i] Department of Geography, McGill University, Montreal, QC, Canada

ARTICLE INFO

Keywords:
Net ecosystem exchange
Methane
Vegetation composition shift
Restoration
Flux
Wetland

ABSTRACT

Peatland rewetting, a management effort to restore water levels in previously drained peatlands, is important for re-establishing the role of these peatlands as carbon (C) sinks. Since rewetted peatlands have a highly variable response to interannual variations in climatic conditions and functional changes, long term studies of C fluxes in these ecosystems are needed. Here, we evaluated the impact of climate variability and functional change on the interannual variability of CO_2 and CH_4 fluxes at Burns Bog, a rewetted temperate bog on the Pacific Coast in Canada, based on five years of eddy covariance measurements. We found that the site alternated between being an annual-scale net CO_2 sink or source, ranging from -32.6 ± 21.5 (±95% CI) to 11.9 ± 15.1 g CO_2–C m^{-2} yr^{-1}, respectively, while consistently being a CH_4 source, ranging from 11.6 ± 0.7 to 18.0 ± 1.6 g CH_4–C m^{-2} yr^{-1}. Over the five-year period, mean annual CH_4 emissions (13.7 ± 2.5 g CH_4–C m^{-2} yr^{-1}; ±SD across years) entirely offset the CO_2 sink (-12.3 ± 20.4 g CO_2–C m^{-2} yr^{-1}), resulting in the site being near-carbon neutral over this period (1.3 ± 23.9 g C m^{-2} yr^{-1}). This finding indicates that excluding CH_4 fluxes from the net C balance results in an overestimation of the net C uptake at this site. Annual CO_2 emissions from the bog were greatest in the year with a dry and warm summer, emphasizing the importance of temperature and water table depth at the bog. Regardless of the greenhouse gas (GHG) metrics (i.e., global warming potential or sustained global warming potential) used in calculating the annual CO_2-eq balance, the site consistently had a positive GHG balance across the study period. Despite mainly acting as a GHG source, the rewetted site will likely have a cooling effect on the climate system over long timescales compared to drained bogs that are large CO_2 sources.

1. Introduction

Peatland ecosystems are known to play a critical role in the global carbon (C) cycle. Most intact peatlands are net CO_2 sinks, collectively sequestering around ~1 Pg C yr^{-1} globally (Frolking et al., 2011). Simultaneously, peatlands are also methane (CH_4) sources, which can influence the overall C and greenhouse gas (GHG) balances of the bog.

To date, many studies have focused on investigating the short-term C balance of peatlands, while only a few have conducted long-term measurements of both CO_2 and CH_4 fluxes (Koehler et al., 2011; Rinne et al., 2018; Roulet et al., 2007). While 1-year studies have found that most intact peatlands are net C sinks, longer-term studies have shown that the magnitude of C uptake varies considerably from year-to-year (Drollinger et al., 2019; Rinne et al., 2018; Ueyama et al., 2020). Some long-term studies have also reported that peatlands can alternate between being C sinks and C sources within a few years depending on environmental conditions (Roulet et al., 2007; Strachan et al., 2016). For drained and restored peatlands, their responses to a changing climate

* Corresponding author.
E-mail address: tin.satriawan@u.nus.edu (T.W. Satriawan).

https://doi.org/10.1016/j.agrformet.2023.109696
Received 25 February 2023; Received in revised form 28 August 2023; Accepted 29 August 2023
Available online 7 September 2023

are even less understood as there are not as many long-term ecosystem scale C flux studies available compared to their intact counterparts (Holl et al., 2020; Nugent et al., 2018; Swenson et al., 2018; Wilson et al., 2016).

One of the most widely studied drivers of CO_2 interannual variability is water table depth (WTD) fluctuation which reflects the severity, timing, and duration of growing season drought and flooding events (Aslan-Sungur et al., 2016; Lund et al., 2012). Summer drought increases CO_2 source strength by enhancing ecosystem respiration (R_{eco}) and suppressing gross primary production (GPP) (Helfter et al., 2015; Lafleur et al., 2003; Lund et al., 2012; McVeigh et al., 2014; Mikhaylov et al., 2019). On the other hand, flooding can decrease net CO_2 uptake by inhibiting GPP through water stress in plants (Aslan-Sungur et al., 2016). Despite these effects, WTD can have a limited impact on the interannual variability of net ecosystem exchange (NEE = R_{eco} - GPP). For example, Pugh et al. (2018) found that the effect of WTD on R_{eco} and GPP canceled each other out, making annual peat temperature the best factor explaining interannual variability in NEE. In another study, Strachan et al. (2016) detected that during low variability of WTD, NEE variability was more sensitive to temperature changes. These differences may be caused by site-specific peat structures and characteristics (Lafleur et al., 2005).

A number of studies have also investigated how functional changes affect interannual variability of CO_2 exchange in peatlands (McVeigh et al., 2014; Teklemariam et al., 2010). Here, functional changes are defined as indirect factors that drive photosynthesis and respiration over time, such as changes in vegetation and microbial composition (Hui et al., 2003). These studies concluded that functional changes can only explain a small portion of the interannual variability of NEE. For example, 5.3% over 10 years at Mer Bleue peatland, Canada (Teklemariam et al., 2010) and 13.7% over 8 years at Glencar Atlantic Blanket Bog, Ireland (McVeigh et al., 2014). However, functional changes in response to rewetting have not been extensively studied.

Additionally, methane emissions from peatlands can be an important component in the net ecosystem carbon balance (NECB). NECB of peatlands typically combines the C exchanged through atmospheric CO_2 and CH_4 fluxes, along with lateral fluxes of C, including dissolved organic C (DOC) and particulate C (PC) (Chapin et al., 2006; D'Acunha et al., 2019; Koehler et al., 2011; Nilsson et al., 2008; Roulet et al., 2007). However, continuous measurements of DOC are often difficult to make in long term studies.

Although many studies have found that interannual variability of the net C balance is driven more by NEE (Rinne et al., 2018; Ueyama et al., 2020), Roulet et al. (2007) demonstrated that including CH_4 fluxes in the calculation is crucial to avoid overestimating the net C sink strength of peatlands. CH_4 fluxes have also been reported to contribute between 5% and 17% of NECB (Nilsson et al., 2008; Nugent et al., 2018), turning peatlands from a net C sink to a C source (Koehler et al., 2011).

As a potent GHG, methane has a global warming potential (GWP) 80, 27, and 7 times that of CO_2 on time scales of 20, 100, and 500 years, respectively (Forster et al. 2021). Thus, including CH_4 fluxes is not only important in the calculation of the net C balance, but it also has a strong impact on the net GHG balance of peatlands (Limpens et al., 2008).

Interannual variability of CH_4 fluxes has been explained by site-specific fluctuations in climate and C inputs. For example, a lowered WTD during summer droughts is known to reduce total annual CH_4 emissions (Drollinger et al., 2019; Goodrich et al., 2015b). The timing of the drought also matters because a low temperature in autumn immediately after the summer drought ends can slow the CH_4 emission recovery (Goodrich et al., 2015b). In another study, Rinne et al. (2018) found a correlation between the growing season GPP and CH_4 flux, suggesting that C input drives interannual variability of CH_4 emission.

This large interannual variability raises the question of whether short-term studies are adequate in characterizing the C and GHG balances of peatlands (Baldocchi et al., 2018). Conducting more long-term C flux measurements is therefore necessary to improve our understanding of the stability of peatlands and their response to disturbances and a changing climate, especially since drivers of CO_2 and CH_4 fluxes vary at different timescales (Wang et al., 2018). Here, we conducted long-term eddy covariance (EC) measurements of ecosystem scale CO_2 and CH_4 fluxes at Burns Bog, a temperate ombrotrophic bog undergoing restoration near Vancouver, Canada, with EC measurements beginning 8 years after rewetting. Our objectives in this study were to: (1) quantify the annual net C and GHG balances of the bog over five years, and (2) to identify the drivers of interannual variability in CO_2 and CH_4 fluxes in the bog.

2. Methods

2.1. Study site

This study was carried out in Burns Bog, an ombrotrophic bog located in Delta, British Columbia, Canada. According to the Köppen regional climate classification, Burns Bog is classified as Csb (warm-summer Mediterranean climate). Between 1981–2010, the mean annual air temperature was 10.6 ± 0.6 °C and mean annual precipitation was 1262.4 mm with only 2% falling as snow based on the nearest weather station data (Richmond Nature Park, 9.13 km from the site) (Environment Canada, 2020). The mean monthly temperature is usually above 16 °C throughout summer, with July being the warmest and the driest month (Environment Canada, 2020).

Historically, disturbance in the area was caused by agricultural activities beginning in the late 1800s, peat harvesting from the 1940s to the mid 1980s, and ongoing encroachment for urban/industrial development. As a result, the peat surface, hydrology, and the bog's original vegetation communities have been greatly impacted. By 2000, Burns Bog had lost approximately 40% of its original area and 1–2 m of its original 4–5 m peat thickness (Hebda et al., 2000; Rigg and Richardson, 1938). In order to protect 2042 ha of the remaining peatland area, the Burns Bog Ecological Conservancy Area (BBECA) was established in 2004. Beginning in 2007, ditch blocking was initiated to raise the water table and restore the bog's ecological integrity (Whitfield et al., 2006).

In 2014, an EC tower for CO_2 measurement was installed in the BBECA and CH_4 measurement was later added in June 2015 (49.1293°N, −122.9849°E; registered as CA-DBB on AmeriFlux Network (Christen and Knox, 2021) (Fig. 1a). The recovering peatland area within the flux footprint had been harvested for peat starting in 1952 and ditches along the northern edge of the area were blocked in 2007 through installation of reinforced peat dams. It represents one of the wettest areas within the BBECA with water table elevations generally high relative to other sites in the conservancy area. The area within the flux footprint is composed of Triggs soil from the soil subgroup Mesic Fibrisol, which mainly consists of decomposed peat with extremely low pH ranging from 3 to 4. The vegetation cover has undergone succession post-harvest and is characterized by stands of white beak-rush (*Rhynchospora alba*) growing above a *Sphagnum* carpet (mainly *Sphagnum tenellum*) (Fig. 1b). Other vegetation found in the area includes bog cranberry (*Oxycoccus palustris*), round-leaved sundew (*Drosera rotundifolia*), tawny cotton-grass (*Eriophorum virginicum*), and great yellow pond lily (*Nuphar polysepala*) (Hebda et al., 2000). *Sphagnum* hummocks are developing and support a variety of low growing ericaceous shrubs.

2.2. Eddy covariance and meteorological measurement

The flux tower was installed in Summer 2014, and concurrent long-term EC measurements of CO_2 and CH_4 fluxes have been carried out since 20 June 2015 on a south-facing tower with EC instruments installed at the 1.8-m height. The three orthogonal wind components (*u*, *v*, and *w*) were measured using a three-dimensional sonic anemometer (CSAT-3, Campbell Scientific Inc. (CSI) Logan, UT, USA, 20 Hz). CO_2 and H_2O mixing ratios were measured using an enclosed-path infrared gas analyzer LI-7200 and CH_4 molar densities were measured with an open-

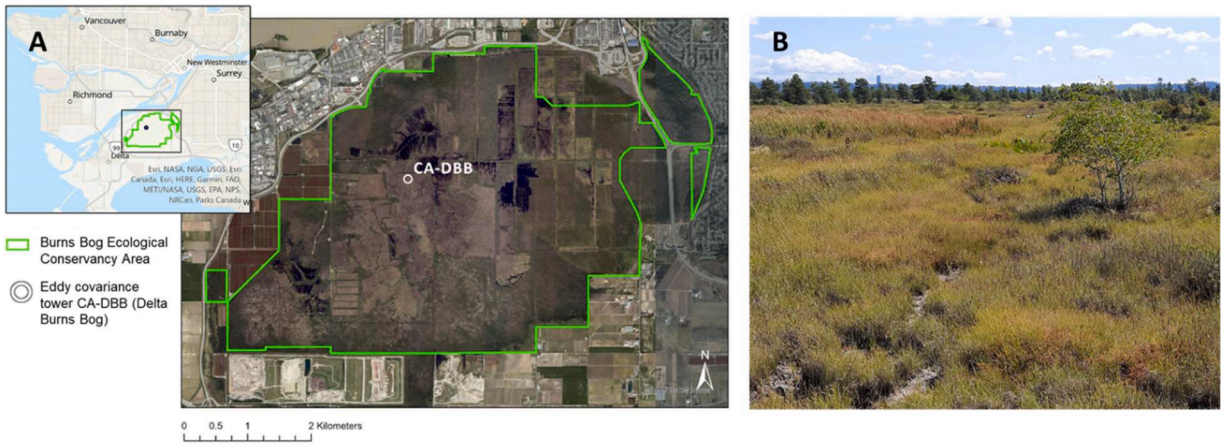

Fig. 1. Study site (a) map of the eddy covariance (EC) tower location in Burns Bog Ecological Conservancy Area (BBECA) near Vancouver, Canada, (b) vegetation cover at the study site (July 2021).

path gas analyzer LI-7700 (both LI-COR Inc. Lincoln, NE, USA, 20 Hz). The EC instruments were equipped with an analyzer interface unit (LI-7550, LI-COR Inc.) and a SmartFlux (LI-COR Inc.) system to enable real-time on-site processing.

Meteorological variables were measured continuously throughout the study period. Incoming and outgoing shortwave and longwave radiation were measured using a net radiometer (CNR1, Kipp and Zonen, Holland), and incoming and outgoing photosynthetically active radiation (PAR) were measured using a pair of quantum sensors (LI-190, LI-COR Inc.) at the 4.25-m height. Air temperature (T_a) and relative humidity (RH) were measured at the 2-m height (HMP-35 A, Vaisala Oyj, Vantaa, Finland) and precipitation was measured 10 m from the EC tower with a tipping bucket rain gage (TR-525 M, Texas Electronics, Dallas, TX, USA). Thermocouples were installed 5 m from the tower to measure soil temperatures at the 5-, 10-, and 50-cm depths (T_s,5 cm, T_s,10 cm and T_s,50 cm). For the WTD measurement, a pressure transducer was installed on 28 July 2015 and was later replaced with a new sensor in summer 2017 (both CS400, CSI). Manual WTD measurements were also conducted once a month from 2018 for calibration purposes. Meteorological measurements were recorded every second and averaged over 30-min periods.

Gaps in the T_a, RH, and wind speed measurements were filled using data from Environment and Climate Change Canada's Delta Burns Bog weather station, located 1.32 km from the site. Incoming shortwave radiation (R_g) and precipitation data were gap-filled using modelled values based on the relationship between the on-site measurements and data from UBC Totem Field weather station, approximately 23 km northwest of the site.

2.3. Flux data processing

Raw flux data measured at 20 Hz were processed in EddyPro (LI-COR Inc.) with an averaging time of 30 min. Statistical tests for raw data screening were conducted to remove spikes, data outside plausible limits, skewness and kurtosis (Vickers and Mahrt, 1997). To correct the sonic anemometer tilt relative to the streamline, the double rotation method was applied (Wilczak et al., 2001). For calculating the turbulent fluctuations, block averaging was used, in which the mean values were removed from the scalar timeseries data. Covariance maximization was then used to correct for time lags arising from sensor separation (Fan et al., 1990). Other corrections applied to the data included the WPL correction to account for the effects of air density changes during the averaging period (Webb et al., 1980) and spectral corrections for low-pass and high-pass filtering (Moncrieff et al., 2004).

The half-hourly fluxes output from EddyPro were further filtered to exclude low-quality records and measurements made under conditions in which EC assumptions were not fulfilled. The half-hourly fluxes were marked with quality flags following a standard developed by Foken et al. (2004), and records flagged as "2" were discarded. Gas analyzer diagnostic flags were also used to discard errors that were typically caused by heavy precipitation and snowfall. Fluxes with spikes in the mean densities, variances, and covariances were removed, along with records when the wind blew through the tower scaffolding (Lee et al., 2021; Nyberg et al., 2022).

Next, the REddyProc package in R was used for friction velocity (u_*) filtering, gap-filling, and partitioning the net CO_2 flux to get continuous NEE, GPP, and R_{eco} records for the entire study period (Wutzler et al., 2018). u_* filtering was done to exclude underestimated fluxes recorded during periods with low turbulent mixing. To determine the u_* threshold for the filter, the moving point method was used (Papale et al., 2006; Reichstein et al., 2005).

Gaps in NEE were filled using the marginal distribution sampling (MDS) approach (Wutzler et al., 2018). Long gaps (>60 days) that were not filled by MDS were then filled using a random forest algorithm using measured vapor pressure deficit (VPD), u_*, T_a, WTD, PAR, R_g, and day of year as predictors (Kim et al., 2020). After gap-filling, NEE was partitioned into its two components (i.e., GPP and R_{eco}) using the nighttime partitioning approach (Reichstein et al., 2005). Using this method, daytime R_{eco} was estimated using daytime T_a based on the relationship between T_a and R_{eco} during nighttime (R_g < 10 Wm^{-2}), and GPP was calculated as R_{eco}–NEE (Reichstein et al., 2005).

Due to limitations of the MDS approach for CH_4 gap-filling (i.e., different biophysical variables input and the more episodic and non-linear nature of CH_4 fluxes), gaps in CH_4 flux were estimated by a random forest algorithm (Kim et al., 2020) using the Caret package in R (Kuhn, 2008). Following Kim et al. (2020) and Knox et al. (2016), we used biophysical variables (i.e., u_*, NEE, latent heat flux (*LE*), sensible heat flux (*H*), R_g, T_a, T_s, 5 cm, T_s, 10 cm, T_s, 50 cm, RH, VPD, WTD) and additional fuzzy variables (i.e., day of year, and sine and cosine waves as a function of time) as inputs.

2.4. Uncertainty analysis

Half-hourly random errors in NEE were calculated using the REddyProc package in R (Wutzler et al., 2018). Aggregation was done by calculating the standard deviation of the annual and seasonal means. To take autocorrelation into account, the aggregated standard deviation was calculated following Zieba and Ramza (2011).

Systematic errors due to MDS gap-filling and u_* threshold selection for NEE, GPP, and R_{eco} were calculated in ReddyProc. The bootstrapping technique was used to generate 200 replicates of the dataset. For each of the replicates, a u_* threshold was estimated, and the results were pooled

together. From the pool of u* thresholds, 39 values from the 2.5th to the 97.5th percentile were extracted. Gap-filling and partitioning were then done repeatedly using each of the u_* threshold estimates (Wutzler et al., 2018). The standard deviation of the 39 estimates was then calculated for each half-hourly value and aggregated to annual and seasonal cumulative values.

For gaps that were filled using the random forest approach (i.e., long gaps in winter 2016 and 2017 NEE, and all periods of CH_4 fluxes), random and gap-filling errors were calculated by generating 20 iterations of random forest estimates. The standard deviation of the 20 estimates were then calculated for each half-hourly value and aggregated to get annual and seasonal sums. For periods of cumulative NEE gap-filled using both MDS and the random forest approach, the standard deviations calculated from these two approaches were added in quadrature.

To get the total uncertainty, random and systematic errors were added in quadrature and presented as the 95% confidence interval. At the annual scale, the contribution of random errors was very small relative to systematic errors and was often negligible.

2.5. Data analysis

The summary of data analyses done in this study along with their purposes and the location of their results are given in Appendix A, Table A1.

2.5.1. Net C balance estimation

We analyzed five years of data starting from winter 2016 through summer 2021. A one-year cycle in this study is defined as the period between 1 October and 30 September the next year. Each period was divided into two seasons: non-growing and growing season. The non-growing season spanned from 1 October to 31 March, while the growing season spanned from 1 April to 30 September. The growing season was defined based on the local climate and followed the approach of Lee et al. (2007) and Nyberg et al. (2022) to allow comparison with these earlier studies conducted at Burns Bog. Additionally, the start and end of carbon uptake of the bog did not exhibit substantial year-to-year fluctuations, typically occurring around the same time each year (i.e., the first week of April – the last week of September).

Net C balance values (in g C m^{-2}) were calculated for the annual, growing season, and non-growing season period each year from the sum of gap-filled half-hourly NEE (g CO_2–C m^{-2}) and CH_4 flux (g CH_4–C m^{-2}). A positive net C balance represented net C loss, while a negative net C balance represented net C uptake by the bog. Note that lateral fluxes were not included in the net C balance estimates for the bog, with implications of this discussed further in the Discussion Section.

2.5.2. GHG balance estimation

The GHG balance was calculated by adding gap-filled values of NEE to CO_2-equivalent emissions of CH_4. To get CO_2-equivalent emissions of CH_4, we used two different metrics: global warming potential (GWP) and sustained-flux global warming potential (SGWP) (Neubauer, 2021; Neubauer and Megonigal, 2015; Forster et al. 2021). Further details are provided in Appendix A, Section A.1.

2.5.3. Relative influence of GPP and R_{eco} on the variability of NEE

To determine the contributions of GPP and R_{eco} to the interannual variability of NEE, their relative influences were calculated following Schaefer et al. (2002):

$$f_{GPP} = \frac{\sigma^2_{GPP}}{(\sigma^2_{GPP} + \sigma^2_{Reco})} \quad (1)$$

$$f_{Reco} = \frac{\sigma^2_{Reco}}{(\sigma^2_{GPP} + \sigma^2_{Reco})} \quad (2)$$

where $f_{GPP}$and $f_{Reco}$are relative influences, and $\sigma^2_{GPP}$and $\sigma^2_{Reco}$are variances of GPP and R_{eco} across years, respectively. Since $f_{Reco} + f_{GPP} = 1$, $f_{Reco} = 0$ indicates that R_{eco} has no influence on interannual NEE variability and $f_{Reco} = 1$ indicates that R_{eco} entirely controls interannual NEE variability. $f_{GPP}$and f_{Reco} were calculated across all years for annual, growing season, and non-growing season timeframes.

2.5.4. Eco-physiological variables

To help explain the eco-physiological responses of the site across years, we also constructed light response curves, calculated surface conductance (*Gs*), and estimated temperature sensitivity (Q10) of R_{eco} and CH_4 flux for each year and season. Further details on the calculations are provided in Appendix A, Section A.2–4.

2.5.5. Yearly multilinear regression (MLR) model

To analyze the variation of daily drivers of C fluxes between years, we determined the significant predictors of daily measured CO_2 and CH_4 fluxes (calculated as daily average of the non-gapfilled half-hourly fluxes) for each year and compared them across years. Two sets of climatic variables (i.e., T_s,5 cm , RH, PAR, VPD, precipitation, P_a, T_a, WTD, and GPP for CH_4; and excluding GPP for CO_2) were used as inputs for forward stepwise multilinear regression (MLR) models for each year. The combination of climatic variables that produced the best model (lowest Akaike information criterion (AIC)) were considered as the significant drivers of daily C fluxes for the particular year.

2.5.6. Homogeneity of slopes (HOS) model

The homogeneity of slopes (HOS) model was used to determine the contribution of direct and indirect effects of environmental conditions on seasonal and interannual variability of CO_2 and CH_4 fluxes (Hui et al., 2003). Using HOS, variability of C fluxes was partitioned into seasonal and interannual components. The interannual components were then further partitioned into direct effects (driven by climatic variability) or indirect effects (driven by functional changes). Further details are provided in Appendix A, Section A.5.

2.5.7. Correlation analysis at the annual scale

To investigate how environmental variables affected annual C fluxes, we conducted a bivariate correlation analysis, with an assumption of a linear relationship between variables. The correlations between cumulative fluxes (i.e., NEE, GPP, R_{eco}, and CH_4 fluxes) and mean annual or seasonal environmental variables (i.e., T_s,5 cm, PAR, precipitation, P_a, T_a, WTD, LUE, Q10) for each year were obtained separately for the growing season, the non-growing season, and the whole year.

3. Results

3.1. Environmental variables

WTD at the study area within the BBECA showed clear seasonality (Fig. 2a), with lower WTD in the growing season (−3.2 ± 3.7 cm; mean ±SD across years; negative values indicate depth below the surface) and higher WTD in the non-growing season (6.2 ± 1.2 cm; positive values indicate height above the surface). This pattern followed precipitation, which is the primary input of water in the bog (Fig. 2b). The 2016–2021 average annual precipitation was 1167.6 ± 89.5 mm and was similar to the 1981–2010 average of 1189 mm. Mean annual T_a from 2016 to 2021 varied between 10.3 and 10.8 °C, with an average of 10.5 °C, which is comparable to the 1981–2010 average of 10.4 °C (Fig. 2c). T_s,5 cm followed a similar seasonal pattern as T_a, with an annual average of 11.4 ± 0.03 °C, a growing season average of 15.8 ± 0.3 °C, and a non-growing season average of 6.9 ± 0.3 °C (Fig. 2d).

The coldest year was 2016–2017, with an annual average T_a of 10.3 °C, which was slightly below the five-year average of 10.5 °C. This was also the wettest year, with annual precipitation and mean annual

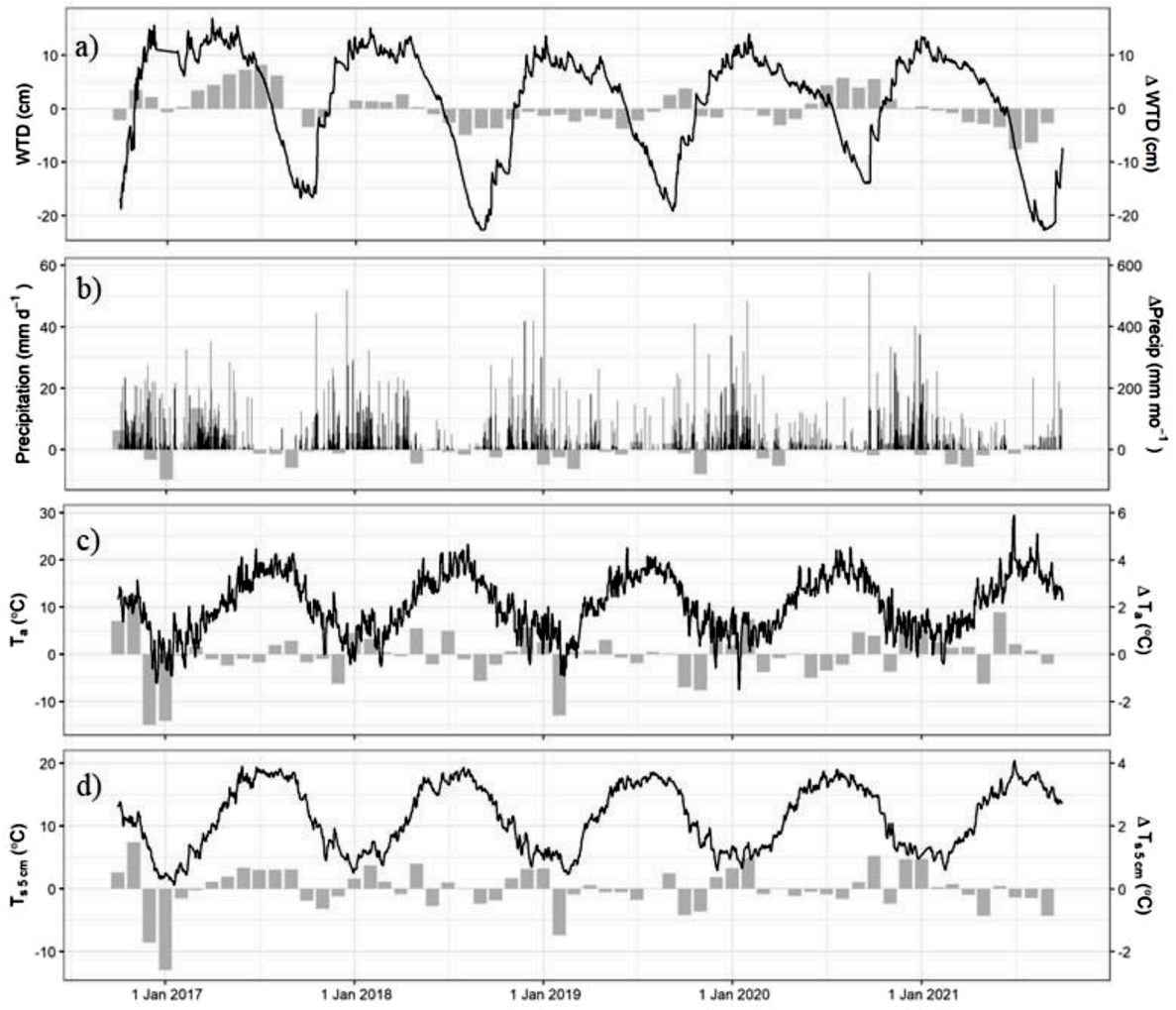

Fig. 2. Daily means (black line) and monthly anomalies (gray bars) for (a) water table depth (WTD), (b) precipitation (c) air temperature (T_a), and (d) soil temperature at the 5-cm depth (T_s,5 cm). Monthly anomalies were calculated as deviations from the monthly means across the five years.

WTD reaching 1296.6 mm and 4.78 cm, respectively. The non-growing season of 2016 started with a warmer fall (October-November), which was followed by a colder winter (December-February) compared to the five-year average (Appendix B, Fig. B.1). Due to higher-than-normal precipitation in spring 2017 (March-May), WTD stayed high in 2017 and only started declining to a level below the surface in mid-July.

The warmest year was 2020–2021 with an annual T_a of 10.9 °C and annual average WTD of −0.1 cm. This is mostly due to growing season anomalies, where three summer months (June to August) had a lower WTD and higher T_a than the five-year averages (Appendix B, Fig. B.1). Maximum daily mean T_a in summer 2021 reached 29 °C, which was ~5 °C higher than the previous years. Additionally, due to low precipitation in spring, this period had an earlier WTD drawdown occurring in early June followed by a rapid decline until mid-July.

3.2. CO_2 exchange

Across the study period, the magnitude of annual NEE and its components varied considerably between years as measured in the study area (Fig. 3, for further details see Appendix B, Table B.1). GPP showed a declining trend throughout the five-year period, ranging from 458.7 ± 30.8 g CO_2–C m^{-2} yr^{-1} (± 95% CI) in the first year to 378.7 ± 16.7 g CO_2–C m^{-2} yr^{-1} in the last year. Similarly, R_{eco} declined from 470.1 ± 38.6 in 2016–2017 to 357.0 ± 12.7 g CO_2–C m^{-2} yr^{-1} in 2019–2020, although it increased again to 390.6 ± 25.2 g CO_2–C m^{-2} yr^{-1} in the last year. Conversely, NEE did not show any clear interannual trend. The site was a weak CO_2 sink in three of the five years, with annual NEE ranging from −26.0 ± 5.5 g CO_2–C m^{-2} yr^{-1} to −32.6 ± 21.5 g CO_2–C m^{-2} yr^{-1}, while in 2016–2017 and 2020–2021 the bog was a CO_2 source, emitting 11.5 ± 16.1 g CO_2–C m^{-2} yr^{-1} and 11.9 ± 15.1 g CO_2–C m^{-2} yr^{-1}, respectively (Table 1).

In the non-growing season, interannual variability in NEE (Fig. 3a) was strongly influenced by R_{eco} (f_{Reco} = 0.90, f_{GPP} = 0.10) due to R_{eco} being more variable than GPP (σ_{Reco} = 27.53 g CO_2–C m^{-2}, σ_{GPP} = 9.0 g CO_2–C m^{-2}). The divergence of daily cumulative wintertime R_{eco} between years (Fig. 3c) was due to higher-than-average R_{eco} in autumn 2016, when monthly R_{eco} reached >45 g CO_2–C m^{-2} in October and November. Conversely, interannual variability in growing season NEE was more strongly influenced by GPP than R_{eco} (f_{GPP} = 0.62, f_{Reco} = 0.38) due to slightly higher variability in growing season GPP than R_{eco} (σ_{GPP} = 29.90 g CO_2–C m^{-2}, σ_{Reco} = 23.26 g CO_2–C m^{-2}). Overall, R_{eco} Fig. 3 was slightly more dominant than GPP in influencing the variability of annual NEE (f_{Reco}= 0.58, f_{GPP} = 0.42).

3.3. CH_4 exchange

Annually, the site was consistently a CH_4 source (Table 1). During the first four years, annual CH_4 fluxes declined from 18.0 ± 1.6 g CH_4–C m^{-2} yr^{-1} to 11.6 ± 0.7 g CH_4–C m^{-2} yr^{-1} before increasing to 13.2 ± 0.8 g CH_4–C m^{-2} yr^{-1} in the last year of the study period (Fig. 3d). CH_4 fluxes

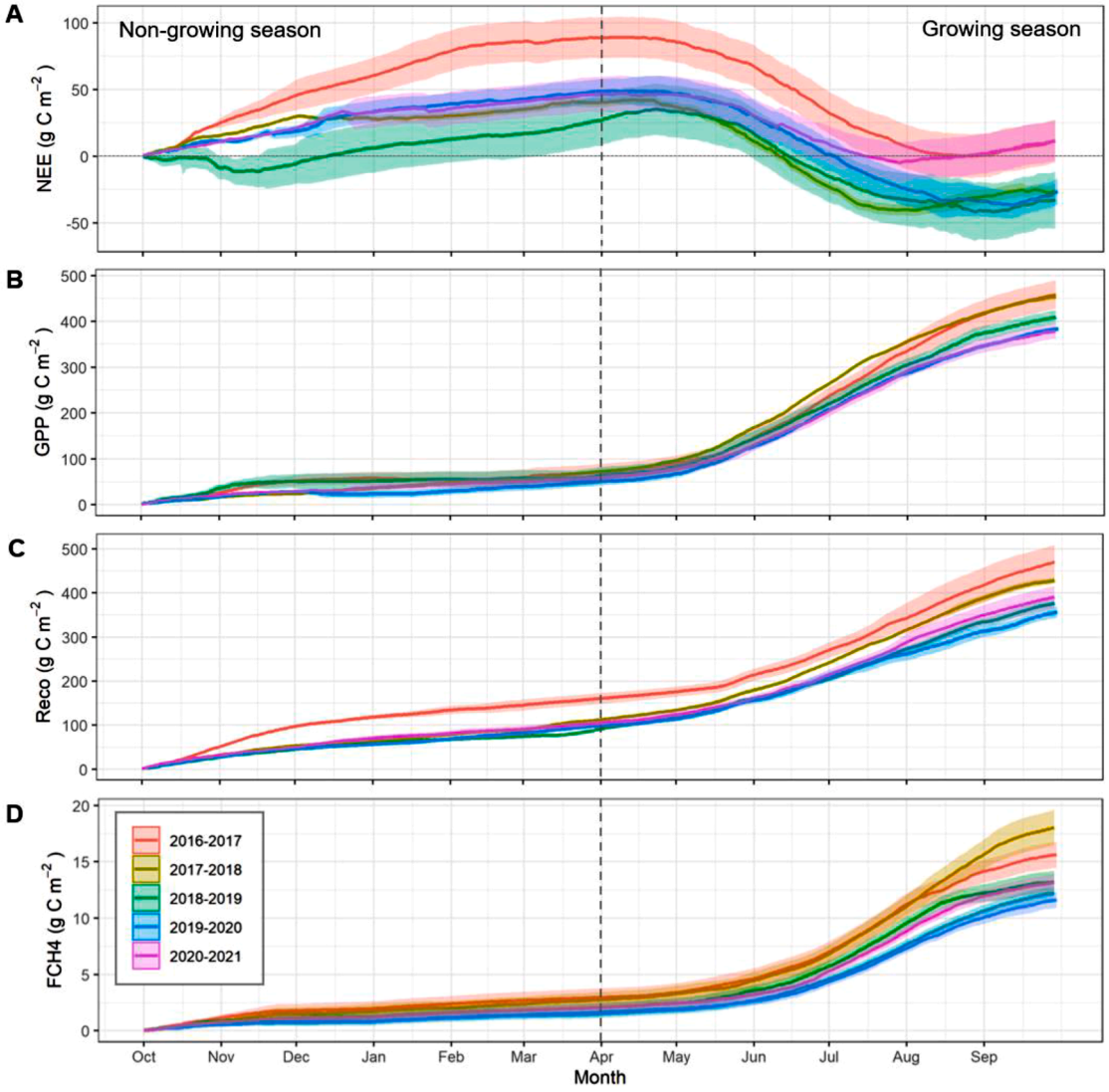

Fig. 3. Cumulative values of (a) net ecosystem exchange (NEE), (b) gross primary production (GPP), (c) ecosystem respiration (R_{eco}), and (c) methane (CH_4). Vertical dashed lines indicate the start of the growing season (1 April); the end of the growing season is 1 October. Uncertainty is presented as 95% CI (shaded areas).

Table 1
Carbon balance of the study site calculated from net ecosystem exchange (NEE) and CH_4 fluxes in g C m^{-2}. Positive values indicate release to the atmosphere (i.e., source), while negative values indicate uptake (sink). Annual and seasonal uncertainty is presented as the 95% CI. Growing season (GS) is from 1 April to 30 September and non-growing season (NGS) is from October to 31 March.

Period	Season	NEE (g CO_2–C m^{-2})			CH_4 flux (g CH_4–C m^{-2})			Net C balance (g C m^{-2})		
2016–2017	Annual	11.5	±	16.1	18.0	±	1.6	29.5	±	16.2
	NGS	88.7	±	15.3	2.8	±	0.7	91.4	±	15.3
	GS	−77.2	±	4.1	15.3	±	1.2	−61.9	±	4.2
2017–2018	Annual	−26.0	±	5.5	13.2	±	1.0	−12.8	±	5.6
	NGS	40.0	±	3.3	2.1	±	0.4	42.1	±	3.3
	GS	−66.0	±	6.7	11.2	±	0.8	−54.8	±	6.8
2018–2019	Annual	−32.6	±	21.5	12.2	±	0.6	−20.4	±	21.5
	NGS	26.6	±	18.8	1.5	±	0.4	28.1	±	18.8
	GS	−59.3	±	5.3	10.7	±	0.5	−48.5	±	5.3
2019–2020	Annual	−26.4	±	9.9	11.6	±	0.7	−14.7	±	10.0
	NGS	48.7	±	9.1	1.6	±	0.3	50.3	±	9.2
	GS	−75.0	±	3.0	10.0	±	0.6	−65.0	±	3.1
2020–2021	Annual	11.9	±	15.1	13.2	±	0.8	25.1	±	15.2
	NGS	46.1	±	13.2	2.1	±	0.3	48.1	±	13.2
	GS	−34.2	±	4.4	11.1	±	0.7	−23.0	±	4.4
Mean ± SD across years	Annual	−12.3	±	20.4	13.7	±	2.5	1.3	±	23.9
	NGS	50.0	±	29.1	2.0	±	0.5	52.0	±	23.7
	GS	−62.3	±	17.3	11.7	±	2.1	−50.7	±	16.7

showed a clear seasonal pattern throughout the years (Table 1), where they were consistently higher in the growing season (11.7 ± 2.1 g CH_4–C m^{-2}) than the non-growing season (2.0 ± 0.5 g CH_4–C m^{-2}). On average, the maxima of CH_4 fluxes occurred in July (3.5 ± 0.5 g CH_4–C m^{-2} $month^{-1}$) and the minima occurred in December (0.1 ± 0.1 g CH_4–C m^{-2} $month^{-1}$).

3.4. Net C balance

The annual net C balance (as the sum of NEE and CH_4 fluxes) within the study area ranged from −20.4 ± 21.5 g C m^{-2} yr^{-1} in 2018–2019 to 29.5 ± 16.2 g C m^{-2} yr^{-1} in 2016–2017 (Table 1). Over the 5 years, the recovering site consistently lost C in the non-growing season (five-year average of 52.0 ± 23.7 g C m^{-2}) while being a C sink in the growing season (five-year average of 50.7 ± 16.7 g C m^{-2}). Averaged over the five years, CH_4 emissions (13.7 ± 2.5 g CH_4–C m^{-2} yr^{-1}) entirely offset NEE (−12.3 ± 20.4 g CO_2–C m^{-2} yr^{-1}), resulting in the site losing an average of 1.3 ± 23.9 g C m^{-2} yr^{-1} to the atmosphere.

3.5. GHG balance

Regardless of the GHG metrics used in the calculation for the 100-year timeframe, the GHG balance of the study area was positive over the five-year period (Table 2). However, the importance of CH_4 decreased over longer time scales, and in 2018–2019, the bog was a small GHG sink for the 500-year timeframe when calculated using GWP (although it remained a weak GHG source when calculated using SGWP).

3.6. Drivers of interannual variability in CO_2

3.6.1. GPP

Across years, there was a consistent decline in annual and growing season GPP (Fig. 3b and Appendix B, Table B.1). We found a significant positive correlation between annual GPP and mean annual VPD (r = 0.90 p<0.05) as shown in Fig. 4a, but no significant correlation with other climatic variables (i.e., T_s5 cm , RH, PAR, precipitation, P_a, T_a, WTD).

To further investigate the interannual drivers of GPP, light response curves were used to demonstrate how half-hourly GPP varied as a function of PAR between years in the growing season (Appendix B, Fig. B.2). The curve fitting parameters of the light response curves (α and P_{max}) declined over the years (Table 3) and they were significantly different across years (p < 0.05). Declining light-saturated photosynthetic capacity (P_{max}) indicates that for a given PAR, maximum photosynthesis was lower in more recent years. As expected, P_{max} also acted as a constraint for GPP, as shown by the significant positive correlation between annual GPP and P_{max} (r = 0.99, p < 0.05) (Fig. 4b). Since light use efficiency (α) describes the initial slope of light response curve, lower α in more recent years indicates a reduced ability of the bog in fixing CO_2 at low light. Based on the correlation analysis, interannual variability of α was influenced by T_s5 cm, in which higher α was associated with higher mean growing season T_s5 cm (r = 0.89, p < 0.05) (Fig. 4c).

To assess the physiological response of the bog plants to water and light availability, we analyzed the relationship between surface conductance (G_s) and VPD, evapotranspiration (ET), and PAR (Appendix B, Fig. B.3). Growing season G_s significantly increased with higher growing season VPD (r = 0.93, p<0.05) and higher growing season ET (r = 0.88, p<0.01). Conversely, G_s significantly decreased with increasing growing season PAR (r = −0.92, p<0.05) (see Appendix B, Fig. B.3).

3.6.2. R_{eco}

We observed no significant bivariate correlation (p>0.05) between annual, growing season, and non-growing season R_{eco} with annual or seasonal mean environmental variables. Therefore, to understand the drivers of interannual variability in R_{eco}, we calculated its temperature sensitivity ($Q10_{RECO}$), which describes the relative increase in R_{eco} per 10 °C rise in soil temperature, from the exponential relationship between daily nighttime NEE and T_s5 cm (Fig. 5). Annual Q10 was the lowest in 2016–2017 ($Q10_{RECO}$ = 3.25) and the highest in 2018–2019 ($Q10_{RECO}$ = 4.63) (see Appendix B, Table B.2).

The year-to-year variability of $Q10_{RECO}$ was mainly attributed to the hydrological conditions of the bog. Based on the correlation analysis, a higher annual $Q10_{RECO}$ was associated with lower annual precipitation (r = −0.95, p<0.05, Fig. 6a) and a lower annual WTD (r = −0.94, p<0.05, Fig. 6b), implying that R_{eco} was less sensitive to T_s5 cm during wetter years. A similar pattern was observed in the non-growing season, in which R_{eco} had a stronger response to T_s5 cm (i.e., higher $Q10_{RECO}$) in years with lower winter WTD (r = −0.87, p<0.01) (Fig. 6c). The $Q10_{RECO}$ –WTD relationship, however, was not significant in the growing season when WTD was close to or below the surface (p>0.01).

3.6.3. NEE

Forward stepwise MLR analysis was used to investigate the year-to-year differences in drivers of daily NEE (Table 4). The performance of the best model varied among years, ranging from an R^2_{adj} value of 0.47 in 2017–2018 to 0.65 in 2016–2017. Generally, PAR and T_s5 cm were better predictors of daily NEE than water-related variables (i.e., WTD, precipitation, and VPD). However, PAR alone consistently underestimated spring daily NEE and overestimated peak summer daily NEE, whereas T_s5 cm alone frequently underestimated late summer and autumn daily NEE. Meanwhile, the inclusion of other variables such as precipitation and VPD only explained an additional 1–2% of the variation in NEE.

To determine the contribution of functional changes and year-to-year climatic variability to interannual variability in NEE, a homogeneity of slopes (HOS) model was used. Based on the model selection process above, T_s5 cm, WTD, and PAR were identified as the three best environmental predictors of NEE for the entire study period. We found that the interactions between year and climatic variables (i.e., the separate slopes model) were not significant (p>0.05), implying that functional changes were not detected. Seasonal climatic variables together with random error contributed to more than half of the variation in NEE (SS_{sc} = 45%, SS_e = 35%), whereas the interannual variation in climatic variables (SS_{ic}, driven primarily by WTD, T_a and PAR) accounted for 20% of year-to-year variability in weekly NEE.

At the annual scale, we found no significant bivariate correlation between annual NEE and mean annual climatic variables (i.e., PAR, T_s5

Table 2
Annual greenhouse gas (GHG) balance of the study site calculated using 100 and 500-year timeframe sustained global warming potential (SGWP) and global warming potential (GWP). Uncertainty is presented as the 95% CI.

Period	$GHG_{SGWP100}$ (g CO_2-eq m^{-2} y^{-1})			$GHG_{SGWP500}$ (g CO_2-eq m^{-2} y^{-1})			GHG_{GWP100} (g CO_2-eq m^{-2} y^{-1})			GHG_{GWP500} (g CO_2-eq m^{-2} y^{-1})		
2016–2017	1192.9	±	111.4	445.7	±	66.1	692.9	±	81.7	215.7	±	60.9
2017–2018	747.7	±	63	200.4	±	27.5	381.5	±	41	31.9	±	22.2
2018–2019	658.2	±	87.3	153.2	±	79.6	320.3	±	81.9	−2.2	±	78.9
2019–2020	646.2	±	56.4	163.9	±	38.8	323.4	±	44.6	15.4	±	37.0
2020–2021	885	±	72.2	338.7	±	57.4	519.4	±	62	170.5	±	56.0

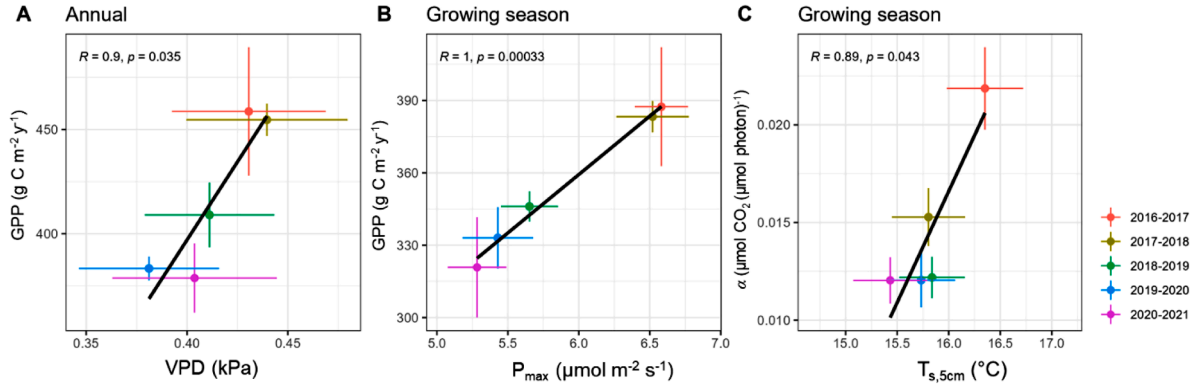

Fig. 4. Correlation analysis between (a) annual gross primary production (GPP) and annual vapor pressure deficit (VPD), (b) growing season GPP and growing season light-saturated photosynthetic capacity (P_{max}), and (c) growing season light use efficiency (α) and growing season soil temperature at 5 cm depth (T_s,5 cm). Error bars indicate 95% confidence interval.

Table 3
Curve fitting parameters, i.e., light use efficiency (α) and light-saturated photosynthetic capacity (P_{max}) for the yearly light response curves.

Period	α (µmol CO_2 (µmol photon)$^{-1}$)	P_{max} (µmol m^{-2} s^{-1})	RMSE (µmol m^{-2} s^{-1})
2016-2017	0.02186	6.58	1.49
2017–2018	0.01527	6.52	1.76
2018–2019	0.01218	5.65	1.50
2019–2020	0.01204	5.43	1.71
2020–2021	0.01203	5.28	1.53

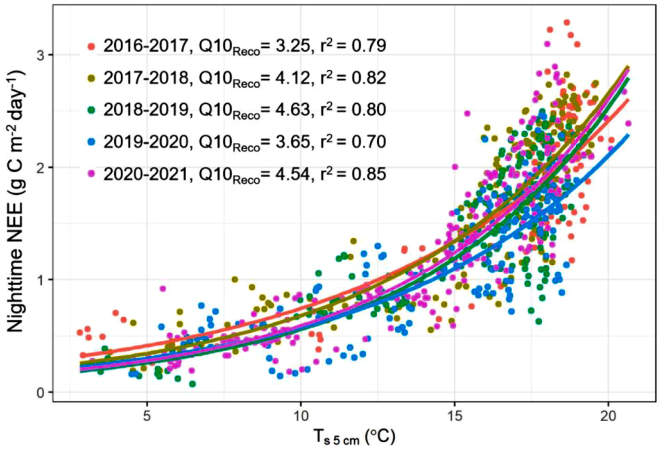

Fig. 5. Nighttime net ecosystem exchange (NEE) as a function of soil temperature at the 5-cm depth (T_s,5 cm) in different years. Data points are daily nighttime NEE which represents non-gap-filled ecosystem respiration (R_{eco}) for the entire annual period; different years are represented by different colors. Curve fitting parameters and root mean square error (RMSE) are shown in Appendix B, Table B.2.

cm, WTD, VPD, RH, precipitation, PA, and T_a). Since climatic variables had no detectable direct effects on interannual variability of NEE, we looked at other related measures, such as the ratio of GPP to R_{eco} (GPP/R_{eco}), and their relationships to environmental variables in the growing and non-growing season. In the growing season, higher GPP/R_{eco} was associated with relatively wetter conditions (i.e., a lower number of days when WTD was deeper than 10 cm below the surface) ($p < 0.05$) (Fig. 7a). An increase in GPP/R_{eco} was also observed with decreasing summer T_a ($r = -0.94$, $p < 0.05$), indicating a greater contribution from R_{eco} in warmer years (Fig. 7b). Thus, years with a warmer and longer dry period in summer had a lower GPP to R_{eco} ratio, and consequently lower growing season net CO_2 uptake.

3.7. Drivers of interannual variability in CH_4

Year-to-year differences in daily drivers of CH_4 fluxes were examined using forward stepwise MLR analysis. The performance of the best model varied among years, ranging from R^2_{adj} value of 0.78 in 2017–2018 to 0.89 in 2018–2019 (Table 4). WTD, GPP, and temperature (i.e., T_a and T_s,5 cm) consistently appeared as the strongest significant predictors for daily CH_4 fluxes in all years. Inclusion of other variables such as PAR, VPD, and P_a only improved the R^2_{adj} values by ~1% and were not able to accurately predict CH_4 flux during its peak period (July-August).

To determine the contribution of functional changes and year-to-year climatic variability to the interannual variability of CH_4 fluxes, the HOS approach was used. A separate slopes model significantly improved CH_4 flux estimates ($p < 0.05$), especially for 2016–2017 (Appendix B, Fig. B.4), indicating that the different CH_4 flux response to climatic variables between years was caused by functional changes. Variations in weekly CH_4 flux were mainly accounted for by seasonal variations in climatic variables and random error (SS_{sc} = 53.8%, SS_e = 23.3%). Interannual variability in WTD, GPP, and T_a accounted for 11.6% of variations in weekly CH_4 flux as SS_{ic}, while functional changes accounted for 11.3% of the variations in weekly CH_4 flux as SS_f.

We also looked at temperature sensitivity ($Q10_{FCH4}$) to investigate the year-to-year variability in the relationship between daily CH_4 flux and T_s,5 cm. $Q10_{FCH4}$ was higher in the growing season ($Q10_{FCH4}$= 22) than in the non-growing season ($Q10_{FCH4}$= 5.7), with an annual $Q10_{FCH4}$ value of 20.5 (Appendix B, Table B.3 and Fig. B.5). Both seasonal and annual $Q10_{FCH4}$ did not differ significantly between years.

4. Discussion

4.1. Interannual variability in CO_2 fluxes

Based on the yearly MLR analyses, daily NEE across the five years was generally controlled by PAR, T_s,5 cm, and WTD and/or precipitation. While seasonal and interannual variations in these three climatic variables contributed to more than half of the interannual variability of weekly NEE (SS_{sc} = 45%, SS_{ic} = 20%), functional changes had an insignificant impact in explaining the interannual variability of weekly NEE based on the HOS results. Here, we interpret functional changes as non-climatic parameters that regulate photosynthesis and respiration (e.g., shifts in vegetation composition, phenology, plant physiology, nutrient status, etc.) following the definition of Hui et al. (2003). In contrast to our observations, McVeigh et al. (2014) reported a significant, although relatively small contribution of functional changes to

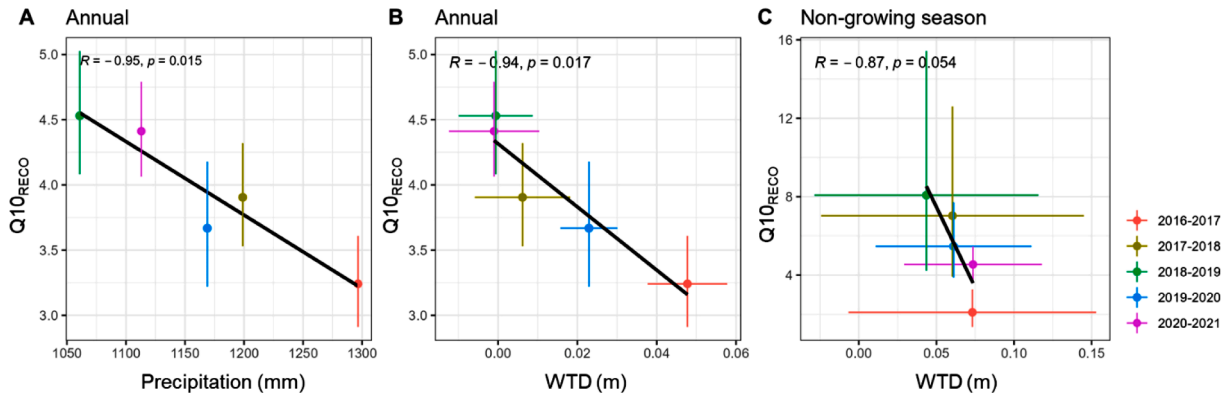

Fig. 6. The relationship between temperature sensitivity of ecosystem respiration ($Q10_{RECO}$) and hydrological variables. (a) Annual $Q10_{Reco}$ against annual precipitation, (b) annual $Q10_{Reco}$ against mean annual WTD, (c) non-growing season $Q10_{Reco}$ against non-growing season WTD. Horizontal error bars indicate 95% confidence interval for the mean of WTD and vertical error bars indicate 95% confidence interval of $Q10_{RECO}$.

Table 4
Forward stepwise multiple linear regression (MLR) model performance for non-gap-filled daily net ecosystem exchange (NEE) and CH_4 flux by year. Variables considered in the analysis are soil temperature at the 5-cm depth (T_s,5 cm), precipitation (Precip), atmospheric pressure (P_a), water table depth (WTD), vapor pressure deficit (VPD), and gross primary production (GPP).

Period	NEE			CH_4		
	Variable	AIC	R^2_{adj}	Variable	AIC	R^2_{adj}
2016–2017	$T_{s,5cm}$	−1.84	0.58	T_a	−839	0.67
	WTD	−20.63	0.64	WTD	−888	0.78
	VPD	−21.19	0.65	GPP	−934	0.85
				PAR	−935	0.85
2017–2018	PAR	21.47	0.43	T_a	−1088	0.61
	$T_{s,5cm}$	12.37	0.46	WTD	−1125	0.69
	WTD	10.58	0.47	$T_{s,5cm}$	−1149	0.73
				GPP	−1181	0.78
				P_a	−1182	0.78
2018–2019	$T_{s,5cm}$	13.06	0.46	WTD	−1461	0.77
	PAR	−28.03	0.57	GPP	−1553	0.86
	Precip	−28.54	0.57	$T_{s,5cm}$	−1600	0.89
2019–2020	PAR	21.48	0.52	T_a	−1232	0.63
	$T_{s,5cm}$	−25.35	0.63	WTD	−1294	0.74
	WTD	−34.63	0.65	GPP	−1331	0.79
	Precip	−35.94	0.65	$T_{s,5cm}$	−1349	0.81
	T_a	−36.52	0.66	P_a	−1352	0.81
2020–2021	PAR	−67.70	0.54	WTD	−1611	0.75
	$T_{s,5cm}$	−99.60	0.60	GPP	−1768	0.87
	VPD	−101.80	0.61	$T_{s,5cm}$	−1775	0.88
	WTD	−102.40	0.61	VPD	−1778	0.88
				P_a	−1780	0.88

variations in NEE at Glencar blanket bog in Ireland. Interestingly, although our HOS results didn't detect a role of functional changes in explaining interannual variability in NEE, we found evidence of a potential vegetation composition shift occurring at this site based on our analysis at the annual scale (as discussed in the next section). In our case, the HOS approach is presumably not sensitive enough to detect functional changes because: (i) GPP and R_{eco} responded similarly to the change, leading to undetectable differences in NEE, (ii) the response was not large enough at the weekly timescale, or (iii) more measurement years are needed to detect the changes.

Annual GPP of the study site across five years (416.9 ± 38.1 g C m^{-2} y^{-1} ; mean ± SD across years) was comparable to the annual GPP of other restored northern bogs (412 to 743 g C m^{-2} y^{-1}) (Nugent et al., 2018; Swenson et al., 2018). In this study, higher annual GPP was associated with higher mean annual VPD (Fig. 4a). VPD could affect GPP through regulating stomatal aperture, in which the opening of stomata leads to higher G_s, thus enhancing CO_2 diffusion into the leaves and increasing photosynthetic rates (Chaves et al., 2004). Depending on climate and plant water use strategy, an increase in VPD can either increase or decrease G_s and ET (Massmann et al., 2019). Some studies have found that high VPD (> 1 kPa) limited GPP due to VPD-induced stomatal closure (Aurela et al., 2007; Cai et al., 2010; Goodrich et al., 2015a; Otieno et al., 2012). At our study site, daily VPD rarely reached 1 kPa, except in the very dry summer of 2021, in which the high VPD only lasted a few days and did not significantly increase the mean growing season VPD. This suggests that our study site falls below the threshold of the inhibitory effect of VPD on GPP, which explains the observed positive GPP – VPD relationship. Similarly, Alekseychik et al. (2017) reported that high VPD favored GPP in a bog in Finland as long as the dry period did not last too long. In this lower range of VPD and wet environment, plants might prioritize photosynthesis over water conservation, as seen by the positive correlation between G_s and VPD (Appendix B, Fig. B.3a) and ET and G_s (Appendix B, Fig. B.3b) at the site. This strategy, however, might only be primarily utilized by vascular plants, as *Sphagnum* mosses lack true stomata and have been suspected to be less responsive to atmospheric water demand (Goodrich et al., 2015a; McAdam et al., 2021).

The magnitude and interannual variability of R_{eco} at this study site (404.6 ± 45.1 g C m^{-2} y^{-1}; mean ± SD across years) was within the range of that reported in other restored temperate peatlands over multiple observation years: from 175.0 ± 100.0 g C m^{-2} y^{-1} at Bellacorick Bog in Ireland (Wilson et al., 2016) to 650.7 ± 28.7 g C m^{-2} y^{-1} at Bois-des-Bel Bog in Canada (Nugent et al., 2018). Although we could not identify any direct primary climatic driver of annual R_{eco}, we found that annual $Q10_{RECO}$ decreased with wetter conditions (higher annual precipitation and WTD) in the bog (Fig. 6a and b). Similarly, Juszczak et al. (2013) reported lower $Q10_{RECO}$ in the year with a higher WTD. It should be noted that in our study, this pattern is particularly observed in the non-growing season when the WTD was above the surface (Fig. 6c). In this case, a higher WTD may have limited the diffusion of CO_2 through the water column, due to water acting as a barrier, which led to lower R_{eco} (Guo et al., 2009; Heinsch et al., 2004; Knox et al., 2018).

When averaged over the five-year period, our site was net CO_2 neutral (−12.3 ± 20.4 g CO_2–C m^{-2}; mean ± SD across years). Annual net CO_2 uptake was generally lower than that of undisturbed northern bogs with multiple years of EC measurements but was within the range of NEE measured in restored peatlands (Fig. 8a). Large between-site and between-year variability of NEE in restored peatlands may be a result of different restoration management practices (Drollinger et al., 2019) and a transition in vegetation community and water table dynamics (Wilson et al., 2016).

Some studies across different ecosystems have found that the variability in NEE is driven more by R_{eco} (Schaefer et al., 2002; Ueyama et al., 2014; Wilson et al., 2016), while others have found GPP to be more influential (Baldocchi et al., 2018; Lund et al., 2010). In our study,

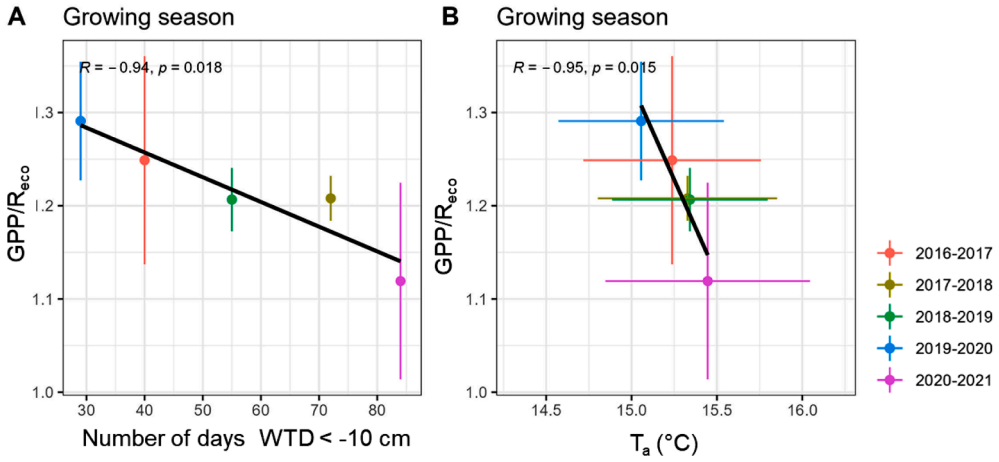

Fig. 7. Growing season correlations between (a) the ratio of gross primary production to ecosystem respiration (GPP/R_{eco}) and the number of days with water table depth (WTD) deeper than 10 cm below the surface, and (b) GPP/R_{eco} and mean air temperature (T_a). Horizontal error bars indicate 95% confidence interval for the mean growing season T_a and vertical error bars indicate 95% confidence interval of GPP/R_{eco}.

we found an almost equal influence of GPP and R_{eco} on interannual variability in NEE. However, we observed different dominant controls in different seasons.

In the growing season, interannual variability in NEE at our study site was mostly driven by the variability in growing season GPP instead of R_{eco}. Lower growing season GPP was associated with lower light use efficiency (α) and lower values for maximum GPP at light saturation (P_{max}) in recent years, indicating a potential shift in vegetation composition from more sedge-dominated to more moss-dominated. Mosses are widely known to have a lower photosynthetic capacity than sedges and other vascular plants on a dry mass or area basis (Green and Lange, 1995; Korrensalo et al., 2016; Laine et al., 2016; Martin and Adamson, 2001; Yuan et al., 2014). Additionally, we observed a decreasing trend of mean growing season soil temperature which coincided with lower α (Fig. 4c), possibly due to the enhanced insulating effect of moss cover on the soil (Chen et al., 2019; Park et al., 2018). In a previous study done in a different area of Burns Bog, Howie et al. (2008) found that the percent cover of *Sphagnum* increased significantly within a year after rewetting. Studies in other restored peatlands also found an increase in moss cover 1 to 19 years after rewetting (Boudreau and Rochefort 2008; Gagnon et al., 2018; Mazzola et al., 2021).

Summer drought has been reported to cause a decrease in net CO_2 uptake by suppressing GPP (Kross et al., 2014; Lund et al., 2012; Shurpali et al., 1995) or enhancing R_{eco} (Aurela et al., 2007; Cai et al., 2010; Drollinger et al., 2019; Lund et al., 2012; Pugh et al., 2018). In this study, we did not find any clear evidence of suppression or enhancement of GPP and R_{eco} during drier and warmer summers. This could be due to the site undergoing a shift in vegetation composition. Differences in the proportion of vascular and moss population can result in contrasting GPP and R_{eco} responses to WTD (Sulman et al., 2010), which suggests that ecosystems in transition may have unclear responses to drier and warmer summers. However, we did observe an overall decrease in GPP/R_{eco} in the summers with higher mean T_a and more days with lower WTD (Fig. 7), suggesting that warmer and drier summers ultimately resulted in a decrease in net CO_2 uptake. The effect of warm and dry summers at the bog was most evident in 2020–2021 period, when the mean growing season WTD reached −7.25 cm and the mean T_a reached 15.45 °C, resulting in the smallest growing season CO_2 uptake among all years (NEE = −34.2 ± 4.4 g C m^{-2}; ± 95% CI) and the lowest growing season GPP (320.86 ± 20.83 g C m^{-2}; ± 95% CI; see Appendix B, Table B.1).

4.2. *Interannual variability in CH_4 fluxes*

Our study site in the BBECA emitted an average of 13.7 ± 2.5 g CH_4–C m^{-2} y^{-1} (± SD across years) across the five-year period, which is comparable to annual CH_4 fluxes of intact and restored peatlands (Fig. 8b). Based on the yearly MLR models, temperature (T_a and T_s5 cm), WTD, and GPP were generally the main drivers of daily CH_4 flux at our study site for all years (Table 4). Although seasonal and interannual variations in these climatic variables contributed to more than half of the interannual variability in weekly CH_4 fluxes (SS_{sc} = 53.8%, SS_{ic} = 11.6), we also found that ~11.3% of interannual variability in CH_4 flux was significantly explained by functional changes. In another study, Rinne et al. (2018) observed a higher contribution of functional changes (~43%) in a boreal fen across the span of 10 years. Here, we interpret functional changes as non-climatic parameters that control CH_4 production, oxidation, and transport (e.g., microbial activity and vegetation phenology). Our finding is supported by Moore et al. (2011), who reported that vegetation cover was a more important driver of CH_4 fluxes than WTD and temperature over a longer time period. Since interannual variability in temperature and water table can affect biomass and the timing of plant growth and senescence (Noyce et al., 2014), plant species inherently carry information on the effects of climatic variables in addition to their own functions (Korrensalo et al., 2021). This indication of the presence of functional changes at the bog aligns with our speculation about shifting vegetation composition (as discussed in Section 4.1). Additionally, Juottonen et al. (2021) reported that methanogen and methanotroph activities (i.e., CH_4 production and CH_4 oxidation, respectively) are sensitive to changes in acidity and moss cover. In acidic conditions created by sphagnum, which dominates vegetation cover in peatlands at older stages of succession, CH_4 production is less, and thus may lead to reduced CH_4 emission (Juottonen et al., 2021; Zhang et al., 2021). This further underlines the importance of functional changes as one of the drivers of CH_4 fluxes.

Although some studies in wetland ecosystems have found higher annual CH_4 fluxes in warmer and/or wetter years (Olson et al., 2013; Drollinger et al., 2019; Knox et al., 2016), we found no significant correlation ($p > 0.05$) between annual or growing season CH_4 fluxes and mean annual environmental variables (WTD, T_a, T_s5 cm). Similarly, Moore et al. (2011), Ueyama et al. (2020), and Rinne et al. (2018) did not find any correlation between annual CH_4 and summer WTD and precipitation.

We found that CH_4 flux sensitivity to soil temperature at this study site (annual $Q10_{FCH4}$ = 20.5) was at the higher end of the $Q10_{FCH4}$ range of peatland ecosystems (1 to 35) estimated from various soil depths and

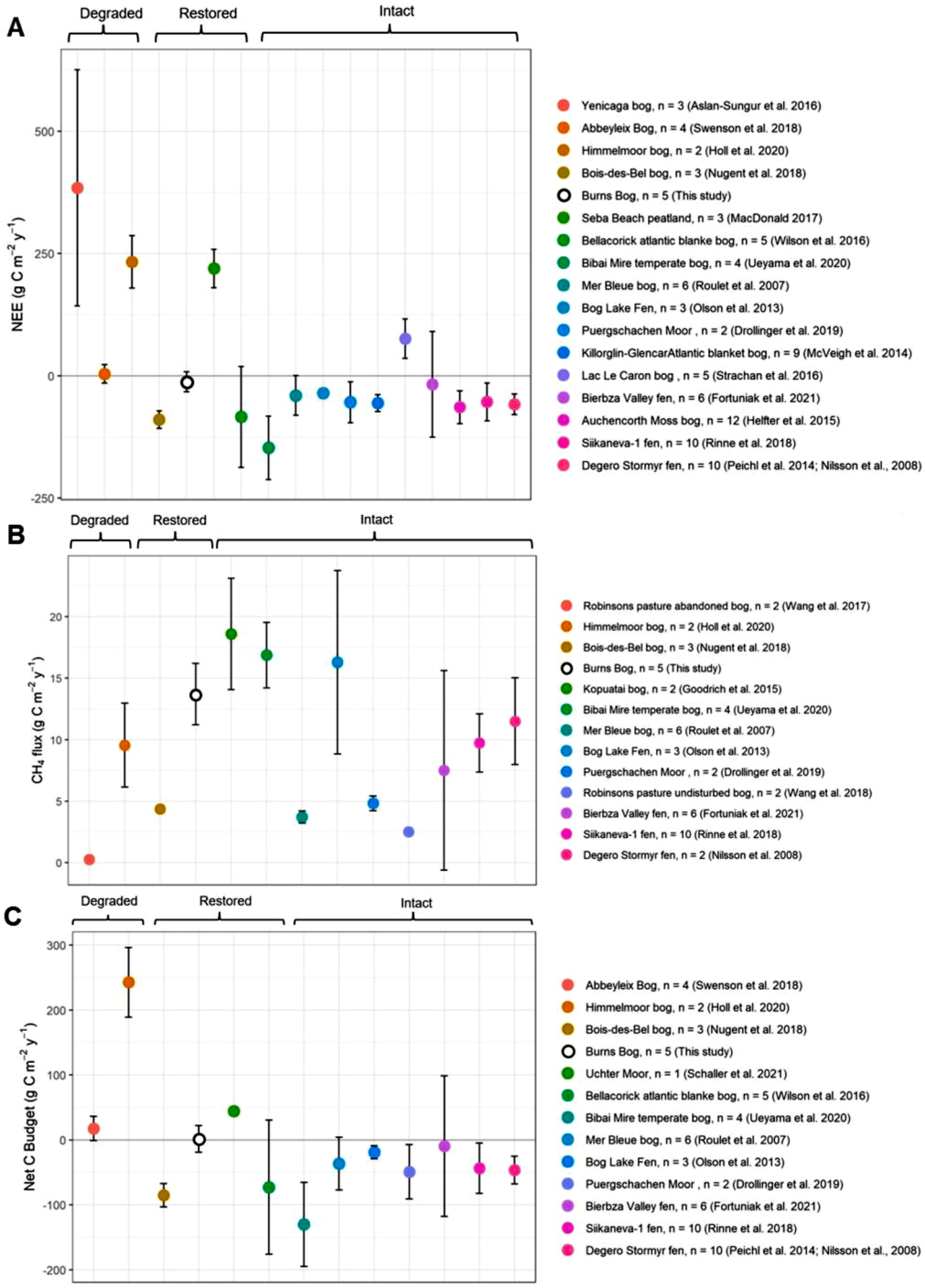

Fig. 8. Comparison of multi-year (>1 year) eddy covariance measurements between degraded, restored, and intact temperate and boreal peatlands (a) for net ecosystem exchange (NEE)(Aslan--Sungur et al., 2016; Drollinger et al., 2019; Fortuniak et al., 2021; Helfter et al., 2015; Holl et al., 2020; MacDonald, 2017; McVeigh et al., 2014; Nugent et al., 2018; Olson et al., 2013; Peichl et al., 2014; Rinne et al., 2018; Roulet et al., 2007; Strachan et al., 2016; Swenson et al., 2018; Ueyama et al., 2020; Wilson et al., 2016); (b) for CH_4 (Drollinger et al., 2019; Fortuniak et al., 2021; Goodrich et al., 2015b; Holl et al., 2020; Nilsson et al., 2008; Nugent et al., 2018; Olson et al., 2013; Rinne et al., 2018; Roulet et al., 2007; Ueyama et al., 2020; Wang et al., 2017, 2018); and (c) for net carbon (C) balance (Drollinger et al., 2019; Fortuniak et al., 2021; Holl et al., 2020; Nilsson et al., 2008; Nugent et al., 2018; Olson et al., 2013; Peichl et al., 2014; Rinne et al., 2018; Roulet et al., 2007; Schaller et al., 2021; Swenson et al., 2018; Ueyama et al., 2020; Wilson et al., 2016). Error bars indicate standard deviations across measurement years.

peatland types (Lupascu et al., 2012; Whalen, 2005). In contrast to findings from Rinne et al. (2018) where $Q10_{FCH4}$ varied interannually from 3.8 to 12 across 11 years, we found no significant difference in $Q10_{FCH4}$ across years in this study ($Q10_{FCH4}$ = 20.5). However, even with variations in $Q10_{FCH4}$, Rinne et al. (2018) reported that growing season soil temperature could not explain interannual variability in CH_4 fluxes in their study site.

The difficulty in assessing drivers of interannual variability at this site may arise from several factors. First, interannual variation in environmental conditions across the five-year study period may not be large enough to produce considerable differences in CH_4 fluxes. The difference in mean annual T_a between the coldest and warmest year at our study site was only 0.3 °C, similar to that of a blanket bog in Ireland where no interannual variability in CH_4 fluxes was observed (Laine et al., 2007). Second, a single variable may not be enough to explain interannual variability in CH_4 fluxes at this site. For example, we speculate that 2016–2017 had the highest annual CH_4 flux due to a combination of several factors, including: (i) higher soil temperatures and GPP (i.e., greater C input) throughout the growing season might have enhanced CH_4 production, (ii) a later timing of water table drawdown and higher spring-summer WTD (i.e., more saturated condition) might have enhanced CH_4 production and plant-mediated transport while reducing the thickness of the methane oxidation zone. However, in 2019–2020, the year with the lowest annual CH_4 emission, we observed a similarly high WTD in the summer but with lower soil temperature. This shows that WTD or soil temperature alone did not necessarily

promote or inhibit annual CH_4 emissions, and that interaction between these, and potentially other, variables is more important.

4.3. Net C balance

When accounting for both net CO_2 (NEE) and CH_4 fluxes, our study site within the bog alternated between an annual C sink and C source, ranging from -20.4 ± 21.5 to 29.5 ± 16.2 to g C m^{-2} y^{-1}. When averaged over the 5-year period, the site was near C neutral, emitting 1.3 ± 23.9 g C m^{-2} y^{-1} (mean $\pm$ SD across five years). Compared to other peatlands, our study site seems to be at a transition stage between drained peatlands that are typically greater C sources and intact peatlands that are typically C sinks (Fig. 8c).

The ratio of annual CH_4 flux to NEE ranged from -0.5 to 1.6 (Table 1), indicating that the inclusion of CH_4 emissions in the net balance either decreased the C sink strength or increased the C source strength of the bog. As a result, CH_4 fluxes at this site are not negligible in terms of the C balance, and excluding them would result in an overestimation of the net C sink strength of the bog.

It is important to note that the net C balances we present here only include CO_2 and CH_4 fluxes and do not represent the full net ecosystem carbon balance (NECB) of the study site. In peatland ecosystems where DOC loss through runoff is reportedly considerable, NECB is commonly estimated from CH_4, CO_2, and lateral transfer of DOC fluxes (Limpens et al., 2008; Roulet et al., 2007). In a previous study by D'Acunha (et al. 2019) at Burns Bog for the 2016–2017 annual cycle, DOC loss in this site (15.6 ± 3.2 g C m^{-2} y^{-1}) made up a significant proportion of the NECB (i.e., $fCO_2 + fCH_4 + fDOC = -29.7 \pm 17.0$ g C m^{-2} y^{-1}). This indicates that only accounting for CH_4 and CO_2 fluxes at Burns Bog may result in underestimation of the annual NECB. However, studies have found that NEE was the most variable component of interannual variability in the net C balance (Nugent et al., 2018; Roulet et al., 2007), suggesting that the exclusion of DOC may be relatively minor when assessing drivers of interannual variability in the overall C balance of the bog.

4.4. GHG balance

To understand the climatic role of our study site, we quantified its annual GHG balance from CH_4 and CO_2 fluxes. It should be noted that we did not include N_2O flux in our calculation of GHG balance. Peatland ecosystems generally have very small N_2O fluxes (Frolking et al., 2011; Hendriks et al., 2007; Wilson et al., 2016), and specifically for our site, Christen et al. (2016) found N_2O fluxes to be negligible.

For the 100-year timeframe, the study site consistently had a positive GHG balance regardless of the metrics used. This reflects the greater potency of CH_4 at shorter time scales (Pugh et al., 2018). For example, although the bog was a net C sink in 2017–2020, the relatively strong radiative forcing of CH_4 made even small emissions of CH_4 significant in the GHG balance during those three years (Lee et al., 2017). Overall, the GHG balance at our study site was within the range of estimates from other peatland sites using the 100-year timeframe (Drollinger et al., 2019; Schaller et al., 2021; Ueyama et al., 2014). (Pugh et al., 2018)

At the 500-year timeframe, the impact of CH_4 becomes less significant in the context of the net GHG balance as CH_4 perturbation lifetime is shorter (12.4 years; Myhre et al., 2013) than that of CO_2 (37 years; Neubauer and Megonigal 2015) (Nyberg et al., 2022). Therefore, when applying the SGWP for the 500-year timeframe, the study site was the weakest GHG source in the 2018–2019 period ($GHG_{SGWP500} = 153.2 \pm 79.6$), which corresponds to the year when the site was the strongest net CO_2 sink.

Despite mainly acting as a net GHG source after 8 to 13 years following rewetting, restoration efforts at our study site have likely provided a net climate benefit relative to leaving the bog drained. It is important to note that the study site already had a considerable organic C stock accumulated as peat at the beginning of the rewetting (Frolking and Roulet, 2007), a factor not taken into account when calculating the GHG balance using GWP or SGWP metrics. To address this limitation and take into account that the lack of rewetting results in large GHG emissions due to continuous peat oxidation (Günther et al., 2020; Leifeld et al., 2019; Nugent et al., 2018), Nyberg et al. (2022) modelled the radiative forcing of two locations in Burns Bog with different rewetting strategies (i.e., active (this site) vs. passive/minimal rewetting). They found that although both re-wetted peatland sites had a positive radiative forcing over century timescales, the lack of restoration would have resulted in significantly greater radiative forcing over time. As such, despite the positive GHG balance, actively rewetting disturbed peatlands can help mitigate climate warming, particularly over long timescales.

4.5. Study limitations

There are some limitations in this study that should be stated. First, data gaps in the winter introduced considerable uncertainty in annual and non-growing season sums, thus limiting our confidence in interpreting non-growing season fluxes and their potential drivers. Second, there is no available vegetation survey within the flux footprint area to confirm any speculation about the nature of vegetation composition changes. Freely available satellite images (e.g., Landsat and MODIS) are also too coarse in their spatial and temporal resolutions, making interpretation difficult. Third, despite the reportedly more important role of soil moisture compared to WTD and precipitation in driving C fluxes (Strack and Price, 2009), we did not have reliable soil moisture measurements during the study period. Finally, although 5 years of data is a long-term dataset for ecosystem-scale GHG flux measurements, additional years of data will allow us to better assess the highly variable biophysical drivers of CO_2 and CH_4 fluxes at this site.

5. Conclusions

Five years of eddy covariance (EC) measurements were conducted at Burns Bog, a temperate ombrotrophic peatland undergoing restoration in British Columbia, Canada, 8 to 13 years after rewetting. As one of the few studies with multiple-year measurements of ecosystem scale CO_2 and CH_4 fluxes in a rewetted peatland (e.g., Nugent et al., 2018; Schaller et al., 2021), our study provides useful insights despite some limitations. Here, we present full annual balances of C fluxes and demonstrate that short-term monitoring is not sufficient to fully characterize the C dynamics of restored peatlands. The variance of seasonal and interannual climatic variables contributed the most to the interannual variability of C fluxes, while functional changes contributed the least and in the case of CO_2, were undetectable. However, we found an indication of functional changes happening at the site (i.e., shift in vegetation composition), as supported by eco-physiological changes over the years. In summary, climatic variability along with functional changes may lead to peatlands switching between C sink and C source within the span of a few years. Furthermore, with predicted increases in the frequency of droughts and heatwaves due to climate change, the re-establishment of the role of restored peatlands as C sinks may be disrupted. For future work, longer term measurements ($>$ 5 years) are necessary to capture the response of peatlands to climate trends and better detect relationships between fluxes and their drivers at the interannual scale.

Declaration of Competing Interest

The authors declare the following financial interests/personal relationships which may be considered as potential competing interests:

Sara Knox, Mark Johnson, Andreas Christen reports financial support was provided by Canada Foundation for Innovation. Sara Knox reports financial support was provided by Metro Vancouver. Sara Knox reports financial support was provided by Natural Sciences and Engineering Research Council of Canada.

Data availability

Data will be made available on request.

Acknowledgment

This study is funded through research contracts between Metro Vancouver and UBC (PI: Knox). Selected equipment was supported by the Canada Foundation for Innovation (Christen, Johnson, and Knox; project number 39738). Knox was also support by an NSERC Discovery Grant (RGPIN-2019-04199) and Alliance Grant (ALLRP 555468-20). We appreciate the technical and logistical support by staff from Metro Vancouver, and assistance of R. Ketler, B. D'acunha, L. Morillas, J. Exler, Y. Kim, S. Russel, M. Nyberg, T.Y. Lu, and J. Skeeter in maintaining the site.

Appendix A Methods

Table A.1

Table A.1
Summary of data analyses done in this study, their purposes, and the location of their results.

Data analysis	Purpose	Location of results
2.5.1 Net C balance estimation	To determine whether the study site was a C sink/source in each year, calculated as the sum of gap-filled NEE (g CO_2–C m^{-2}) and CH_4 flux (g CH_4–C m^{-2})	Section 3.4 (Table 1, Appendix B Table B.1)
2.5.2 GHG balance estimation	To determine the CO_2-equivalent GHG fluxes in each year	Section 3.5 (Table 2)
2.5.3 Relative influence of GPP and R_{eco} on the variability of NEE	To identify the contribution of GPP and R_{eco} to the interannual variability in NEE for annual, growing season, and non-growing season timeframes.	Section 3.2
2.5.4 Eco-physiological variables		
A.2 Light response curves	To demonstrate how the GPP-PAR relationship, as indicated by the light use efficiency (α) and light-saturated photosynthetic capacity (P_{max}), changes across years. To detect potential shifts in vegetation composition	Section 3.6.1 (Fig. 4b and c, Table 3, Appendix B Fig. B.2)
A.3 Surface conductance	To assess the physiological response of vegetation to water and light availability	Section 3.6.1 (Appendix B Fig. B.3)
A.4 Temperature Sensitivity of R_{eco} and FCH_4	To demonstrate how the relationship between temperature and R_{eco} and CH_4 differ between years	Section 3.6.2 (Fig. 5, Appendix B Table B.2, Fig. 6) Section 3.7 (Appendix B Table B.3 and Fig. B.5)
2.5.5 Yearly multilinear regression (MLR) model	To identify year-to-year differences in daily drivers of NEE and CH_4 fluxes	Section 3.6.3 (Table 4) Section 3.7 (Table 4)
2.5.6 Homogeneity of slopes (HOS) model	To determine the primary climatic drivers of NEE and CH_4 across all years To partition the interannual variability in weekly NEE and CH_4 into four components: seasonal variations in climatic variables, interannual variations in climatic variables, functional changes, and random error	Section 3.6.3 Section 3.7 (Appendix B, Fig. B.4)
2.5.7 Correlation analysis at the annual scale	To investigate the influence of environmental variables on growing season, non-growing season, and annual C fluxes To investigate the relationship between environmental variables and eco-physiological variables	Section 3.6.1 (Fig. 4, Appendix B Fig. B.3) Section 3.6.2 (Fig. 6) Section 3.6.3 (Fig. 7)

A.1. GHG balance estimation

Calculations of annual GHG budgets using a 100 and 500-year GWP were done using the equations below:

$$GHG\ budget_{GWP100} = m_{CO_2} F_{CO_2} + \left(m_{CH_4} F_{CH_4} \times GWP_{100}\right) \quad (A.1)$$

$$GHG\ budget_{GWP500} = m_{CO_2} F_{CO_2} + \left(m_{CH_4} F_{CH_4} \times GWP_{500}\right) \quad (A.2)$$

Where m_{CO2} and m_{CH4} refer to the molecular mass of CO_2 (44.01 g mol^{-1}) and CH_4 (16.04 g mol^{-1}) respectively; F_{CO2} and F_{CH4} refer to CO_2 and CH_4 fluxes in mol m^{-2} yr^{-1}; GWP_{20} , GWP_{100}, and GWP_{500} are the GHG metrics that describe the radiative effect of a pulse of CH_4 emission relative to a pulse emission of an equal mass of CO_2 for 20, 100, and 500 year timeframes, respectively. Here, we used a GWP_{20} value of 79.7, GWP_{100} of 27.0, and GWP_{500} of 7.2 (Forster et al. 2021).

The annual GHG balances from using the 100 and 500-year SGWP values were calculated as follows:

$$GHG\ budget_{SGWP100} = F_{CO2-seq} + \left(F_{CH4} \times SGWP_{100}\right) \quad (A.3)$$

$$GHG\ budget_{SGWP500} = F_{CO2-seq} + \left(F_{CH4} \times SGWP_{500}\right) \quad (A.4)$$

$$F_{CO2-seq} = \left(F_{CO_2} + F_{CH_4}\right) \times m_{CO_2} \quad (A.5)$$

where $SGWP_{20}$ (= 96), $SGWP_{100}$ (= 45), and $SGWP_{500}$ (= 14), are the GHG metrics that describe the radiative effect of a sustained emission of CH_4 relative to sustained sequestration of an equal mass of CO_2 over 20 and 100 year timeframes, respectively; and $F_{CO2\text{-}seq}$ refers to annual net CO_2 sequestration (negative value for sequestration, positive value for emission) calculated as the sum of annual NEE and the amount of carbon lost as CH_4 (Neubauer and Megonigal 2015).

A.2 Light Response Curves

Light response curves were used to demonstrate how growing season GPP varied as a function of half-hourly PAR between years. The GPP-PAR relationship was represented by a rectangular hyperbola function (Thornley and Johnson 1990; Frolking et al., 1998) as follows:

$$GPP = \frac{\alpha \times PAR \times P_{max}}{\alpha \times PAR + P_{max}} \quad (A.6)$$

where α is the slope of increase in GPP at low light levels, also known as the light-use efficiency (μmol CO_2/μmol photon) and P_{max} is the maximum GPP at high light levels (μmol m^{-2} s^{-1}).

To compare the year-to-year differences of the GPP-PAR relationship, we fitted two light response curves: one model where α and P_{max} were identical between years and another model where α and P_{max} varied between years. An F-test was then used to compare the two models. If the null hypothesis was rejected ($p<0.05$) we concluded that at least one of the years had significantly different α and P_{max}.

A.3. Surface Conductance (G_s)

Surface conductance (G_s) (m s^{-1}) was calculated by inverting the Penman-Monteith equation (Baldocchi and Meyers 1998; Ryu et al., 2008) to get:

$$\frac{1}{G_s} = \frac{1}{G_a}\left\{\frac{\frac{s}{\gamma}(Rn - G) + \frac{\rho C_p G_a VPD}{\gamma}}{LE} - \frac{s}{\gamma}\right\} - 1 \quad (A.7)$$

where G_a is the aerodynamic conductance (m s^{-1}), s is the slope of relation between saturation vapor pressure and air temperature (kPa K^{-1}), γ is the psychrometric constant, R_n is the net radiation (W m^{-2}), G is the ground heat flux (W m^{-2}), ρ is the air density (kg m^{-3}), C_p is the specific heat of air (J kg^{-1} K^{-1}), VPD is the vapor pressure deficit (kPa) and LE is the latent heat flux (W m^{-2}). G_a was calculated as follows:

$$\frac{1}{G_a} = \frac{1}{G_{a,m}} + \frac{1}{G_b} \quad (A.8)$$

$$\frac{1}{G_{a,m}} = \frac{u}{u_*^2} \quad (A.9)$$

$$\frac{1}{G_b} = \frac{kB^{-1}}{ku_*} \quad (A.10)$$

where $G_{a,m}$ is the aerodynamic conductance for momentum transfer, G_b is the laminar boundary layer conductance (m s^{-1}), u is the mean wind speed (m s^{-1}), u_* is the friction velocity (m s^{-1}), k is the von Karman constant (0.4), and kB^{-1} is a constant that depends on the surface roughness. Here, we used $kB^{-1} = 2$ for short grass following (Garratt and Hicks 1973).

A.4. Temperature Sensitivity of R_{eco} and FCH_4

To analyze how C fluxes respond to variations in soil temperature, we calculated the temperature sensitivity (Q10) of R_{eco} and CH_4 flux. Q10 describes the relative increase in daily R_{eco} or CH_4 flux per 10 °C rise in daily soil temperature. Here, we estimated Q10 for the growing season, non-growing season, and the entire year of measurements separately for R_{eco} and CH_4 flux using the following equation:

$$Q10_{Reco} = e^{10b_{Reco}} \quad (A.11)$$

$$Q10_{FCH4} = e^{10b_{FCH4}} \quad (A.12)$$

where b_{RECO} and b_{FCH4} are the fitting parameters obtained from the function relating T_s,5 cm to R_{eco} and CH_4 flux (FCH_4), respectively. The relationship between R_{eco} and T_s,5 cm were modeled using a linear fit of the logarithmically transformed nighttime NEE (Equation (A.13), while the relationship between CH_4 flux and T_s,5 cm was modeled using an exponential function due to the presence of negative CH_4 fluxes (Equation (A.14) as follows:

$$ln\left(NEE_{nighttime}\right) = A + b_{Reco}T_{s,5cm} \quad (A.13)$$

$$FCH_4 = ae^{b_{FCH4}T_{s,5cm}} \quad (A.14)$$

where A and b_{RECO} are the intercept and slope of the linear model of $ln(NEE_{nighttime})$, a is the initial CH_4 flux at T_s,5 cm = 0, and b_{FCH4} is the growth of the exponential function of T_s,5 cm.

We fitted the temperature response of R_{eco} and CH_4 flux for each year separately and for all years combined and compared the two estimates using F-test. If the null hypothesis was rejected ($p<0.05$) we concluded that at least one of the years had a significantly different Q10 relative to the Q10 for the full period.

A.5. Homogeneity of slopes (HOS) model

For the model input, we calculated the weekly averages of daily sums of non-gapfilled CO_2 and CH_4 fluxes (only taking daily sums with more than 30% of half-hourly values available), and the weekly averages of climatic variables to attenuate daily fluctuations and maximize use of observations with gaps (D. Hui et al. 2003; T.A. Teklemariam et al. 2010; P. McVeigh et al. 2014). For modeling CO_2, we used a set of climatic variables (i.e., T_s,5 cm, RH, PAR, VPD, precipitation, P_a, T_a and WTD) as predictors. Similarly, we used the same set of predictor variables for modeling CH_4 with the addition of GPP.

Before conducting the HOS analysis, we first identified which predictor variables were relevant to include in the model. To do this, we combined measurements from all years and performed a forward stepwise multiple linear regression (MLR) analysis using the set of climatic variables as the independent variables and CO_2 or CH_4 flux as the dependent variable. We selected a combination of a maximum of three relevant variables that gave the lowest akaike information criterion (AIC) for CO_2 and CH_4 flux each. PAR, T_s,5 cm and WTD were found to be relevant predictors for CO_2, while WTD, GPP, and T_a were found to be relevant predictors for CH_4.

Using the selected predictors, a HOS model that considered the interaction of climatic variable and year was constructed:

$$Y_{ij} = a + \sum_{k=1}^{m} b_k X_{ijk} + \sum_{k=1}^{m} b_{ik} X_{ijk} + e_{ij} \quad (A.15)$$

where i is the i^{th} year; j is the j^{th} day of a year; k is the k^{th} predictor variable; Y_{ij} is the observed dependent variable (CO_2 or CH_4 flux) in i^{th} year and j^{th} day; X_{ijk} is the observed predictor variable in i^{th} year and j^{th} day for the k^{th} predictor; b_k is the slope of regression for the k^{th} predictor; b_{ik} is the slope of the interaction term between the k^{th} predictor and the i^{th} year; e_{ij} is the random error associated with Y_{ij}.

To investigate the presence of functional changes, we tested the null hypothesis (H_0: $b_{ik} = 0$) for all years against the alternative hypothesis (H_1: $b_{ik} \neq 0$) for any of the years. If H_0 could not be rejected, the model had a single slope to predict C fluxes from climatic variables for all years, indicating that functional changes were not significant. Equation (A.15) was then simplified to a single-slope MLR model:

$$Y_{ij} = a + \sum_{k=1}^{m} b_k X_{ijk} + e_{ij} \quad (A.16)$$

If H_0 was rejected, the relationship between climatic variables and C fluxes varied between years. The varying responses were assumed to be caused by the presence of functional changes. Equation (A.15) was then simplified to a separate-slopes MLR model:

$$Y_{ij} = a + \sum_{k=1}^{m} b_{ik} X_{ijk} + e_{ij} \quad (A.17)$$

If functional change was detected, variations of observed C fluxes were classified into direct effects of seasonal climatic variability, direct effects of interannual climatic variability, functional changes (indirect effects), and random errors. Statistically, the classification was done by partitioning the sum of squares (SS) of the total deviation (SS_T) into sum of squares of functional changes (SS_f), sum of squares of the interannual climatic variability (SS_{ic}), sum of squares of the seasonal climatic variability (SS_{sc}), and sum of squares of error (SS_e) as follows:

$$SS_T = SS_f + SS_{ic} + SS_{sc} + SS_e \quad (A.18)$$

SS_f, SS_e, SS_{sc}, and SS_{ic} were calculated respectively by:

$$SS_f = \sum_{i=1}^{y} \sum_{j=1}^{n} \left(\widehat{Y}_{ij}^{'} - \widehat{Y}_{ij} \right)^2 \quad (A.19)$$

$$SS_e = \sum_{i=1}^{y} \sum_{j=1}^{n} \left(Y_{ij} - \widehat{Y}_{ij}^{'} \right)^2 \quad (A.20)$$

$$SS_{ic} = \sum_{i=1}^{y} \sum_{j=1}^{n} \left(\widehat{Y}_{ij} - \overline{Y}_{\cdot j} \right)^2 \quad (A.21)$$

$$SS_{sc} = \sum_{i=1}^{y} \sum_{j=1}^{n} \left(\overline{Y}_{\cdot j} - \overline{Y} \right)^2 \quad (A.22)$$

where $\widehat{Y}_{ij}$ is the estimated C flux from Equation (A.16); $\widehat{Y}_{ij}^{'}$ is the estimated C fluxes from Equation (A.17); $\overline{Y}$ is the mean of all estimated C fluxes; $\overline{Y}_{\cdot j}$ is the mean of estimated C fluxes across all years on the j^{th} day.

If functional change was not significant in the model, SS_T was partitioned into three components only:

$$SS_T = SS_{ic} + SS_{sc} + SS_e \quad (A.23)$$

where SS_e, SS_{sc}, and SS_{ic} were calculated using Equation (A.20), (A.21), (A.22), respectively.

Appendix B

Fig. B.1, Fig. B.2, Fig. B.3, Fig. B.4, Fig. B.5,
Table B.1, Table B.2, Table B.3

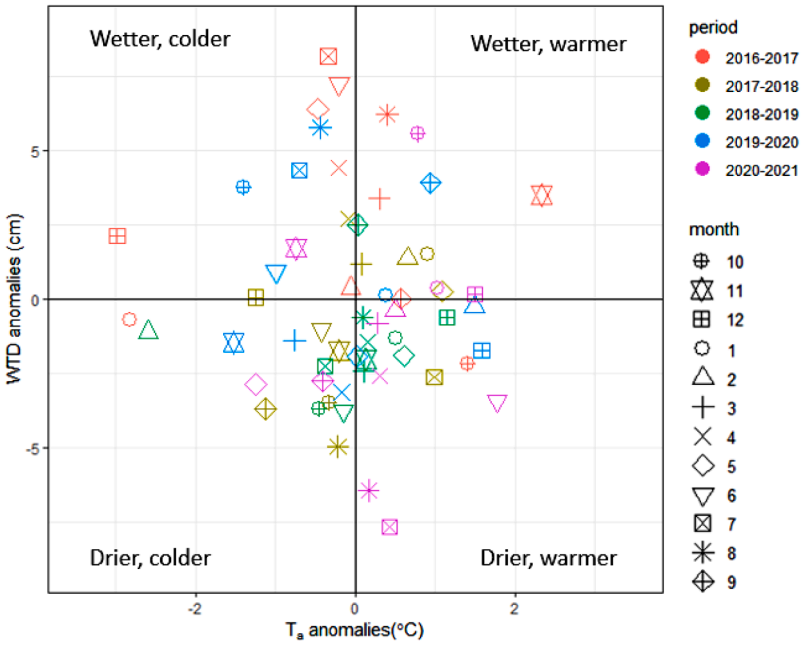

Fig. B.1. Monthly water table depth (WTD) and air temperature (T_a) anomalies. Anomalies were calculated by comparing individual months to their monthly averages across the five-year study period.

Table B.1
Annual, non-growing season (NGS), and growing season (GS) net ecosystem exchange (NEE), gross primary production (GPP), and ecosystem respiration (R_{eco}) of Burns Bog in g CO_2-C m^{-2} and their uncertainties (± 95% CI)

Period	Season	NEE (g C m^{-2})	GPP (g C m^{-2})	R_{eco} (g C m^{-2})
2016-2017	Annual	11.49±16.10	458.66±30.82	470.14±38.63
	NGS	88.67±15.27	71.23±17.24	159.90±12.42
	GS	-77.18±4.07	387.43±24.66	310.24±28.49
2017-2018	Annual	-25.98±5.46	454.63±7.75	428.65±7.09
	NGS	40.00±3.31	71.35±4.21	111.35±3.19
	GS	-65.98±6.72	383.28±6.50	317.30±5.43
2018-2019	Annual	-32.61±21.48	409.00±15.51	376.40±9.63
	NGS	26.64±18.84	62.93±18.00	89.58±1.95
	GS	-59.25±5.30	346.07±6.25	286.82±8.24
2019-2020	Annual	-26.38±9.92	383.35±5.73	356.97±12.67
	NGS	48.67±9.15	50.28±8.84	98.95±3.58
	GS	-75.05±3.00	333.06±12.75	258.02±13.11
2020-2021	Annual	11.91±15.14	378.73±16.65	390.64±25.20
	NGS	46.08±13.24	57.87±11.41	103.95±8.50
	GS	-34.17±4.36	320.86±20.83	286.69±23.86
Mean±SD across years	Annual	-12.31±20.38	416.87±38.12	404.56±38.12
	NGS	50.01±29.13	62.73±9.02	112.75±9.02
	GS	-62.33±17.31	354.14±29.89	291.81±29.89

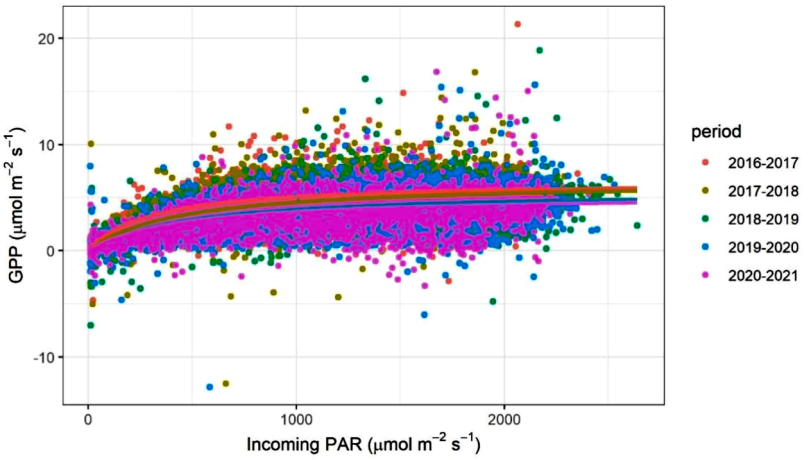

Fig. B.2. Comparison of light response curves (i.e., Gross primary production (GPP) as a function of photosynthetically active radiation (PAR)) between years. The data points are half-hourly non-gap-filled growing season GPP.

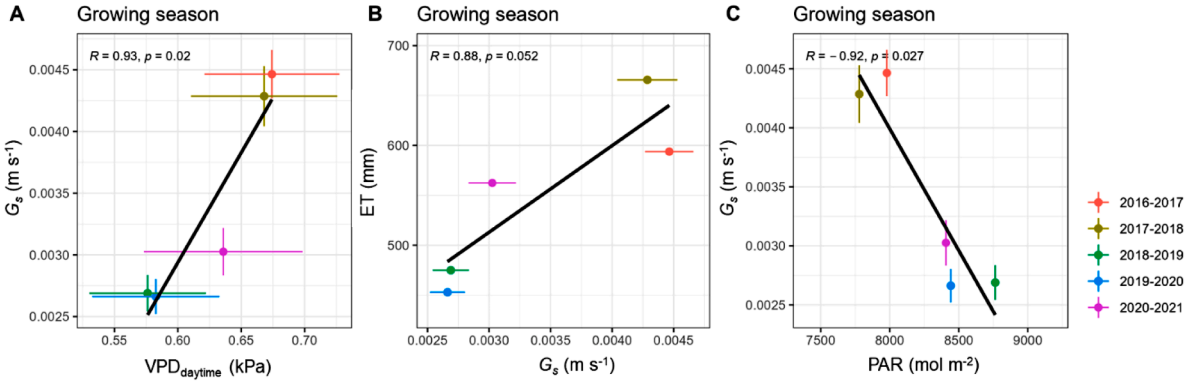

Fig. B.3. Growing season correlations between (a) surface conductance (G_s) and daytime vapor pressure deficit (VPD), (b)G_s and evapotranspiration (ET), and (c) G_s and incoming photosynthetically active radiation (PAR). Error bars represent 95% confidence interval of the variables.

Table B.2
Comparison of curve fitting parameters (A and b) and temperature sensitivity of ecosystem respiration ($Q10_{RECO}$), and the model goodness-of-fit between years.

Period	*A*	b_{RECO}	$Q10_{RECO}$	r^2	RMSE (g C m^{-2} D^{-1})
2016–2017	0.24	0.12	3.25	0.79	0.27
2017–2018	0.17	0.14	4.12	0.82	0.27
2018–2019	0.12	0.15	4.63	0.80	0.30
2019–2020	0.16	0.13	3.68	0.70	0.33
2020–2021	0.13	0.15	4.54	0.85	0.27

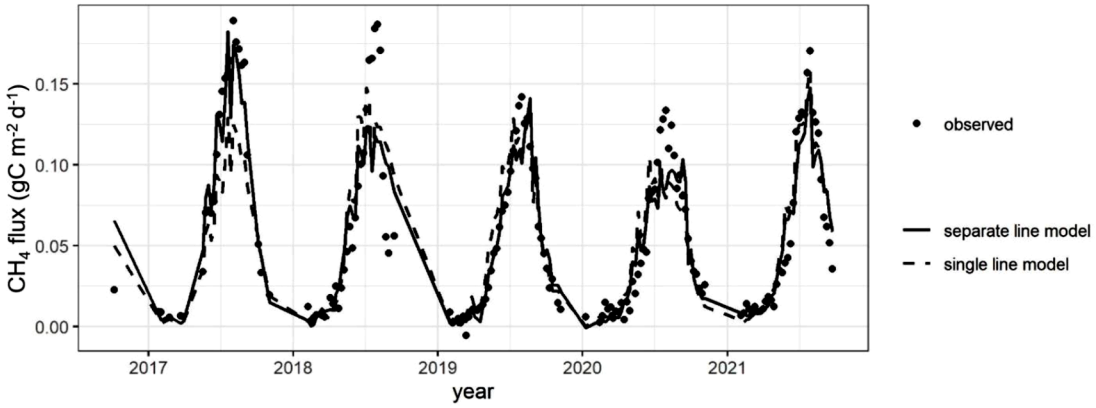

Fig. B.4. Comparison of single-slope and separate-slopes models for estimating weekly mean daily CH_4 flux constructed from weekly mean daily water table depth (WTD), gross primary production (GPP), and air temperature (T_a).

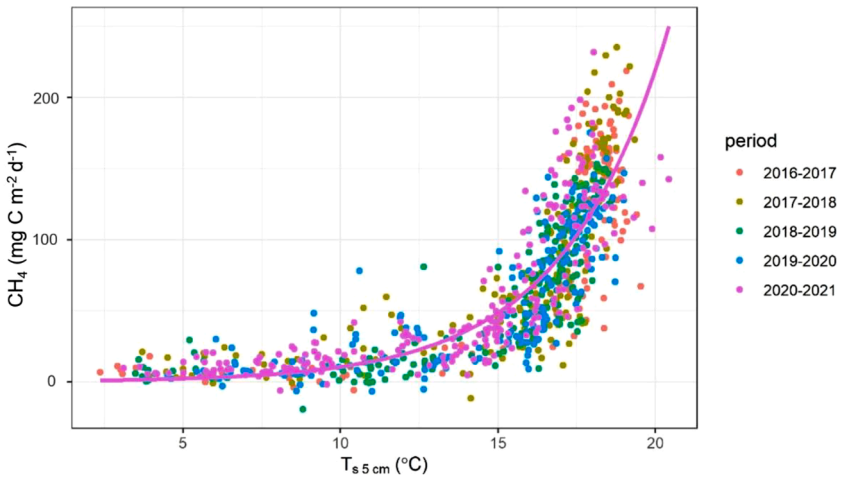

Fig. B.5. Daily CH_4 fluxes as a function of soil temperature at 5 cm (T_s,5 cm) in different years. Data points are non-gapfilled daily CH_4 fluxes for the entire annual period; different years are represented by different colors.

Table B.3
Comparison of curve fitting parameter (a and b) and temperature sensitivity of CH_4 flux ($Q10_{CH4}$), and the model goodness-of-fit between years (RMSE).

Period	*a*	b_{FCH4}	$Q10_{CH4}$	RMSE (g C m^{-2} $_D$$^{-1}$)
Annual	0.0005	0.30	20.48	0.029
Non-growing season	0.0032	0.17	5.69	0.011
Growing season	0.0005	0.31	22.03	0.032

References

Alekseychik, P., Mammarella, I., Karpov, D., Dengel, S., Terentieva, I., Sabrekov, A., Glagolev, M., Lapshina, E., 2017. Net ecosystem exchange and energy fluxes measured with the eddy covariance technique in a western Siberian bog. Atmos. Chem. Phys. 17 (15), 9333–9345. https://doi.org/10.5194/acp-17-9333-2017.

Aslan-Sungur, G., Lee, X., Evrendilek, F., Karakaya, N., 2016. Large interannual variability in net ecosystem carbon dioxide exchange of a disturbed temperate peatland. Sci. Total Environ. 554–555, 192–202. https://doi.org/10.1016/j.scitotenv.2016.02.153.

Aurela, M., Riutta, T., Laurila, T., Tuovinen, J.P., Vesala, T., Tuittila, E.S., Rinne, J., Haapanala, S., Laine, J., 2007. CO2 exchange of a sedge fen in southern Finland - The impact of a drought period. Tellus, Ser. B: Chem. Phys. Meteorol. 59, 826–837. https://doi.org/10.1111/j.1600-0889.2007.00309.x.

Baldocchi, D., Chu, H., Reichstein, M., 2018. Inter-annual variability of net and gross ecosystem carbon fluxes: a review. Agric. For. Meteorol. 249 (November 2016), 520–533. https://doi.org/10.1016/j.agrformet.2017.05.015.

Baldocchi, D., Meyers, T., 1998. On using eco-physiological, micrometeorological and biogeochemical theory to evaluate carbon dioxide, water vapor and trace gas fluxes over vegetation: a perspective. Agric. For. Meteorol. 90, 1–25. https://doi.org/10.1016/S0168-1923(97)00072-5.

Boudreau, S., Rochefort, L., 2008. Plant establishment in restored peatlands : 10-years monitoring of sites restored from 1995 to 2003. In: Proceedings of the 13th International Peat Congress: After Wise Use–The Future of Peatlands, pp. 362–366.

Cai, T., Flanagan, L.B., Syed, K.H., 2010. Warmer and drier conditions stimulate respiration more than photosynthesis in a boreal peatland ecosystem: analysis of automatic chambers and eddy covariance measurements. Plant Cell Environ. 33 (3), 394–407. https://doi.org/10.1111/j.1365-3040.2009.02089.x.

Chapin, F.S., Woodwell, G.M., Randerson, J.T., Rastetter, E.B., Lovett, G.M., Baldocchi, D.D., Clark, D.A., Harmon, M.E., Schimel, D.S., Valentini, R., Wirth, C., Aber, J.D., Cole, J.J., Goulden, M.L., Harden, J.W., Heimann, M., Howarth, R.W., Matson, P.A., McGuire, A.D., Schulze, E.D., 2006. Reconciling carbon-cycle concepts, terminology, and methods. Ecosystems 9 (7), 1041–1050. https://doi.org/10.1007/s10021-005-0105-7.

Chaves, M.M., Osorio, J., Pereira, J.S., 2004. Water use efficiency and photosynthesis. In: Bacon, M.A. (Ed.), Water Use Efficiency in Plant Biology. Blackwell Publishing Ltd, pp. 42–74.

Chen, S., Yang, Z., Liu, X., Sun, J., Xu, C., Xiong, D., Lin, W., Li, Y., Guo, J., Yang, Y., 2019. Moss regulates soil evaporation leading to decoupling of soil and near-surface air temperatures. J. Soil. Sedim. 2903–2912. https://doi.org/10.1007/s11368-019-02297-4.

Christen, A., Jassal, R.S., Black, T.A., Grant, N.J., Hawthorne, I., Johnson, M.S., Lee, S.-C., Merkens, M., 2016. Summertime greenhouse gas fluxes from an urban bog undergoing restoration through rewetting. Mire. Peat 17. https://doi.org/10.19189/MaP.2015.OMB.207. UNSP 03.

Christen, A., Knox, S., 2021. AmeriFlux BASE CA-DBB Delta Burns Bog (Version 2-5). AmeriFlux AMP. https://doi.org/10.17190/AMF/1543378. </Dataset>.

D'Acunha, B., Morillas, L., Black, T.A., Christen, A., Johnson, M.S., 2019. Net ecosystem carbon balance of a peat bog undergoing restoration: integrating CO2 and CH4 fluxes from Eddy covariance and aquatic evasion with DOC drainage fluxes. J. Geophys. Res.: Biogeosci. 124 (4), 884–901. https://doi.org/10.1029/2019JG005123.

Drollinger, S., Maier, A., Glatzel, S., 2019. Interannual and seasonal variability in carbon dioxide and methane fluxes of a pine peat bog in the Eastern Alps, Austria. Agric. For. Meteorol. 275, 69–78. https://doi.org/10.1016/j.agrformet.2019.05.015. May.

Environment Canada. (2020). *Canadian Climate Normals 1981-2010: richmond Nature Park*.

Fan, S., Wofsy, S.C., Bakwin, P.S., Jacob, D.J., Fitzjarrald, D.R., 1990. Atmosphere-Biosphere Exchange of CO2 and O3 in the Central Amazon Tropical Forest, 95, pp. 16851–16864.

Foken, T., Gockede, M., Mauder, M., Mahrt, L., Amiro, B., Munger, J.W., 2004. Post-field data quality control. In: Lee, X., Massman, W.J., Law, B. (Eds.), Handbook of Micrometeorology. Kluwer Academic, pp. 181–208.

Fortuniak, K., Pawlak, W., Siedlecki, M., Chambers, S., Bednorz, L., 2021. Temperate mire fluctuations from carbon sink to carbon source following changes in water table. Sci. Total Environ. 756 https://doi.org/10.1016/j.scitotenv.2020.144071.

Forster, P., Storelvmo, T., Armour, K., Collins, W., Dufresne, J.L., Frame, D., Lunt, D.J., Mauritsen, T., Palmer, M.D., Watanabe, M., Wild, M., Zhang, H., 2021. The earth's energy budget, climate feedbacks, and climate sensitivity. Climate Change 2021: The Physical Science Basis. Contribution of Working Group I to the Sixth Assessment Report of the Intergovernmental Panel On Climate Change. Cambridge University Press, pp. 923–1054. https://doi.org/10.1017/9781009157896.009.923.

Frolking, S., Roulet, N.T., 2007. Holocene radiative forcing impact of northern peatland carbon accumulation and methane emissions. Glob. Chang. Biol. 13 (5), 1079–1088. https://doi.org/10.1111/j.1365-2486.2007.01339.x.

Frolking, S., Bubier, J.L., Moore, T.R., et al., 1998. Relationship between ecosystem productivity and photosynthetically active radiation for northern peatlands. Glob. Biogeochem. Cycle. 12, 115–126. https://doi.org/10.1029/97GB03367.

Frolking, S., Talbot, J., Jones, M.C., Treat, C.C., Kauffman, J.B., Tuittila, E.S., Roulet, N., 2011. Peatlands in the Earth's 21st century climate system. Environ. Rev. 19 (1), 371–396. https://doi.org/10.1139/a11-014.

Gagnon, F., Rochefort, L., Lavoie, C., 2018. Spontaneous revegetation of a peatland in manitoba after peat extraction: diversity of plant assemblages and restoration perspectives. Botany 96 (11), 779–791. https://doi.org/10.1139/cjb-2018-0109.
Garratt, J.R., Hicks, B.B., 1973. Momentum, heat and water vapour transfer to and from natural and artificial surfaces. Q. J. R. Meteorol. Soc. 99, 680–687. https://doi.org/10.1002/qj.49709942209.
Goodrich, J.P., Campbell, D.I., Clearwater, M.J., Rutledge, S., Schipper, L.A., 2015a. High vapor pressure deficit constrains GPP and the light response of NEE at a Southern Hemisphere bog. Agric. For. Meteorol. 203, 112–123. https://doi.org/10.1016/j.agrformet.2015.01.001.
Goodrich, J.P., Campbell, D.I., Roulet, N.T., Clearwater, M.J., Schipper, L.A., 2015b. Overriding control of methane flux temporal variability by water table dynamics in a Southern Hemisphere, raised bog. J. Geophys. Res.: Biogeosci. 120, 819–831. https://doi.org/10.1002/2014JG002844.Received.
Green, T.G.A., Lange, O.L, 1995. Photosynthesis in poikilohydric plants: a comparsion of lichens and bryophytes. In: Schulze, E.D., Caldwell, M.M. (Eds.), Ecophysiology of Photosynthesis. Springer, pp. 319–341.
Günther, A., Barthelmes, A., Huth, V., Joosten, H., Jurasinski, G., Koebsch, F., Couwenberg, J., 2020. Prompt rewetting of drained peatlands reduces climate warming despite methane emissions. Nat. Commun. 11 (1), 1–5. https://doi.org/10.1038/s41467-020-15499-z.
Guo, H., Noormets, A., Zhao, B., Chen, J., Sun, G., Gu, Y., Li, B., Chen, J., 2009. Tidal effects on net ecosystem exchange of carbon in an estuarine wetland. Agric. For. Meteorol. 149 (11), 1820–1828. https://doi.org/10.1016/j.agrformet.2009.06.010.
Hebda, R.J., Gustavson, K., Golinski, K., Calder, A.M., 2000. Burns Bog Ecosystem Review Synthesis Report for Burns Bog, Fraser River Delta, South-western British Columbia. Canada(Issue March).
Heinsch, F.A., Heilman, J.L., McInnes, K.J., Cobos, D.R., Zuberer, D.A., Roelke, D.L., 2004. Carbon dioxide exchange in a high marsh on the Texas Gulf Coast: effects of freshwater availability. Agric. For. Meteorol. 125 (1–2), 159–172. https://doi.org/10.1016/j.agrformet.2004.02.007.
Helfter, C., Campbell, C., Dinsmore, K.J., Drewer, J., Coyle, M., Anderson, M., Skiba, U., Nemitz, E., Billett, M.F., Sutton, M.A., 2015. Drivers of long-term variability in CO2 net ecosystem exchange in a temperate peatland. Biogeosciences 12 (6), 1799–1811. https://doi.org/10.5194/bg-12-1799-2015.
Hendriks, D.M.D., Van Huissteden, J., Dolman, A.J., Van Der Molen, M.K., 2007. The full greenhouse gas balance of an abandoned peat meadow. Biogeosciences 4 (3), 411–424. https://doi.org/10.5194/bg-4-411-2007.
Holl, D., Pfeiffer, E.M., Kutzbach, L., 2020. Comparison of eddy covariance CO2 and CH4 fluxes from mined and recently rewetted sections in a northwestern German cutover bog. Biogeosciences 17 (10), 2853–2874. https://doi.org/10.5194/bg-17-2853-2020.
Howie, S., Munson, T., Hebda, R., Jeglum, J., Whitfield, P., Dakin, R., 2008. Restoration of Burns Bog, Delta, British Columbia, Canada. In: After Wise Use – The Future of Peatlands, Proceedings of the 13th International Peat Congress: Pristine Mire Landscapes, 1, pp. 51–55.
Hui, D., Luo, Y., Katul, G., 2003. Partitioning interannual variability in net ecosystem exchange between climatic variability and functional change. Tree Physiol. 23 (7), 433–442. https://doi.org/10.1093/treephys/23.7.433.
Juottonen, H., Kieman, M., Fritze, H., Hamberg, L., Laine, A.M., Merilä, P., Peltoniemi, K., Putkinen, A., Tuittila, E.S., 2021. Integrating decomposers, methane-cycling microbes and ecosystem carbon fluxes along a peatland successional gradient in a land uplift region. Ecosystems. https://doi.org/10.1007/s10021-021-00713-w.
Juszczak, R., Humphreys, E., Acosta, M., Michalak-Galczewska, M., Kayzer, D., Olejnik, J., 2013. Ecosystem respiration in a heterogeneous temperate peatland and its sensitivity to peat temperature and water table depth. Plant Soil 366 (1–2), 505–520. https://doi.org/10.1007/s11104-012-1441-y.
Kim, Y., Johnson, M.S., Knox, S.H., Black, T.A., Dalmagro, H.J., Kang, M., Kim, J., Baldocchi, D., 2020. Gap-filling approaches for eddy covariance methane fluxes: a comparison of three machine learning algorithms and a traditional method with principal component analysis. Glob. Chang. Biol. 26 (3), 1499–1518. https://doi.org/10.1111/gcb.14845.
Knox, S.H., Windham-Myers, L., Anderson, F., Sturtevant, C., Bergamaschi, B., 2018. Direct and indirect effects of tides on ecosystem-scale CO2 exchange in a brackish tidal marsh in Northern California. J. Geophys. Res.: Biogeosci. 123 (3), 787–806. https://doi.org/10.1002/2017JG004048.
Knox, Sara H., Matthes, J.H., Sturtevant, C., Oikawa, P.Y., Verfaillie, J., Baldocchi, D., 2016. Biophysical controls on interannual variability in ecosystem-scale CO2 and CH4 exchange in a California rice paddy. J. Geophys. Res.: Biogeosci. 121, 978–1001. https://doi.org/10.1002/2015JG003247.
Koehler, A.K., Sottocornola, M., Kiely, G., 2011. How strong is the current carbon sequestration of an Atlantic blanket bog? Glob. Chang. Biol. 17 (1), 309–319. https://doi.org/10.1111/j.1365-2486.2010.02180.x.
Korrensalo, A., Hájek, T., Vesala, T., Mehtätalo, L., Tuittila, E.S., 2016. Variation in photosynthetic properties among bog plants. Botany 94 (12), 1127–1139. https://doi.org/10.1139/cjb-2016-0117.
Korrensalo, A., Mammarella, I., Alekseychik, P., Vesala, T., Tuittila, E.S., 2021. Plant mediated methane efflux from a boreal peatland complex. Plant Soil. https://doi.org/10.1007/s11104-021-05180-9. *0123456789*.
Kross, A., Roulet, N., Moore, T., Lafleur, P., Humphreys, E., Seaquist, J., Flanagan, L., Aurela, M., 2014. Phenology and its role in carbon dioxide exchange processes in northern peatlands. J. Geophys. Res.: Biogeosci. 119, 1370–1384. https://doi.org/10.1002/2014JG002666.Received.
Kuhn, M., 2008. Building predictive models in R using the caret package. J. Stat. Softw. 28 (5), 1–26. https://doi.org/10.18637/jss.v028.i05.
Lafleur, P.M., Moore, T.R., Roulet, N.T., Frolking, S., 2005. Ecosystem respiration in a cool temperate bog depends on peat temperature but not water table. Ecosystems 8 (6), 619–629. https://doi.org/10.1007/s10021-003-0131-2.
Lafleur, P.M., Roulet, N.T., Bubier, J.L., Frolking, S., Moore, T.R., 2003. Interannual variability in the peatland-atmosphere carbon dioxide exchange at an ombrotrophic bog. Glob. Biogeochem. Cycle. 17 (2), 1–14. https://doi.org/10.1029/2002gb001983.
Laine, A.M., Tolvanen, A., Mehtätalo, L., Tuittila, E.S., 2016. Vegetation structure and photosynthesis respond rapidly to restoration in young coastal fens. Ecol. Evol. 6 (19), 6880–6891. https://doi.org/10.1002/ece3.2348.
Laine, A., Wilson, D., Kiely, G., Byrne, K.A., 2007. Methane flux dynamics in an Irish lowland blanket bog. Plant Soil 299 (1–2), 181–193. https://doi.org/10.1007/s11104-007-9374-6.
Lee, S.C., Black, T.A., Nyberg, M., Merkens, M., Nesic, Z., Ng, D., Knox, S.H., 2021. Biophysical impacts of historical disturbances, restoration strategies, and vegetation types in a peatland ecosystem. J. Geophys. Res.: Biogeosci. 126 (10), 1–20. https://doi.org/10.1029/2021JG006532.
Lee, S.C., Christen, A., Black, A.T., Johnson, M.S., Jassal, R.S., Ketler, R., Nesic, Z., Merkens, M., 2017. Annual greenhouse gas budget for a bog ecosystem undergoing restoration by rewetting. Biogeosciences 14 (11), 2799–2814. https://doi.org/10.5194/bg-14-2799-2017.
Leifeld, J., Wüst-Galley, C., Page, S., 2019. Intact and managed peatland soils as a source and sink of GHGs from 1850 to 2100. Nat. Clim. Chang. 9 (12), 945–947. https://doi.org/10.1038/s41558-019-0615-5.
Limpens, J., Berendse, F., Blodau, C., Canadell, J.G., Freeman, C., Holden, J., Roulet, N., Rydin, H., Schaepman-Strub, G., 2008. Peatlands and the carbon cycle: from local processes to global implications - a synthesis. Biogeosciences 5 (5), 1475–1491. https://doi.org/10.5194/bg-5-1475-2008.
Lund, M., Christensen, T.R., Lindroth, A., Schubert, P., 2012. Effects of drought conditions on the carbon dioxide dynamics in a temperate peatland. Environ. Res. Lett. 7 (4) https://doi.org/10.1088/1748-9326/7/4/045704.
Lund, M., Lafleur, P.M., Roulet, N.T., Lindroth, A., Christensen, T.R., Aurela, M., Chojnicki, B.H., Flanagan, L.B., Humphreys, E.R., Laurila, T., Oechel, W.C., Olejnik, J., Rinne, J., Schubert, P., Nilsson, M.B., 2010. Variability in exchange of CO_2 across 12 northern peatland and tundra sites. Glob. Chang. Biol. 16 (9), 2436–2448. https://doi.org/10.1111/j.1365-2486.2009.02104.x.
Lupascu, M., Wadham, J., Hornibrook, E., Pancost, R., 2012. Temperature sensitivity of methane production in the permafrost active layer at Stordalen, Sweden: a comparison with non-permafrost Northern Wetlands. Arct. Antarct. Alp. Res. 44 (4), 469–482. https://doi.org/10.1657/1938-4246-44.4.469.
MacDonald, S.M., 2017. Carbon gas Exchange at a Recently Restored Peatland in Alberta, Canada. McGill University. *McGill University* (Issue December).
Martin, C.E., Adamson, V.J., 2001. Photosynthetic capacity of mosses relative to vascular plants. J. Bryol. 23 (4), 319–323. https://doi.org/10.1179/jbr.2001.23.4.319.
Massmann, A., Gentine, P., Lin, C., 2019. When does vapor pressure deficit drive or reduce evapotranspiration? J. Adv. Model. Earth Syst. 11 (10), 3305–3320. https://doi.org/10.1029/2019MS001790.
Mazzola, V., Perks, M.P., Smith, J., Yeluripati, J., Xenakis, G., 2021. Seasonal patterns of greenhouse gas emissions from a forest-to-bog restored site in northern Scotland: influence of microtopography and vegetation on carbon dioxide and methane dynamics. Eur. J. Soil Sci. 72 (3), 1332–1353. https://doi.org/10.1111/ejss.13050.
McAdam, S.A.M., Duckett, J.G., Sussmilch, F.C., Pressel, S., Renzaglia, K.S., Hedrich, R., Brodribb, T.J., Merced, A., 2021. Stomata: the holey grail of plant evolution. Am. J. Bot. 108 (3), 366–371. https://doi.org/10.1002/ajb2.1619.
McVeigh, P., Sottocornola, M., Foley, N., Leahy, P., Kiely, G., 2014. Meteorological and functional response partitioning to explain interannual variability of CO_2 exchange at an Irish Atlantic blanket bog. Agric. For. Meteorol. 194, 8–19. https://doi.org/10.1016/j.agrformet.2014.01.017.
Mikhaylov, O.A., Zagirova, S.V., Miglovets, M.N., 2019. Seasonal and inter-annual variability of carbon dioxide exchange at a boreal peatland in north-east European Russia. Mire. Peat 24, 1–16. https://doi.org/10.19189/MaP.2017.OMB.293.
Moncrieff, J., Clement, R., Finnigan, J., Meyers, T., 2004. Averaging, detrending, and filtering of Eddy covariance time series. In: Lee, X., Massman, W.J., Law, B. (Eds.), Handbook of Micrometeorology. Kluwer Academic, pp. 7–32. https://doi.org/10.1007/1-4020-2265-4_1.
Moore, T.R., De Young, A., Bubier, J.L., Humphreys, E.R., Lafleur, P.M., Roulet, N.T., 2011. A multi-year record of methane flux at the Mer Bleue Bog, Southern Canada. Ecosystems 14 (4), 646–657. https://doi.org/10.1007/s10021-011-9435-9.
Myhre, G., Shindell, D., Bréon, F.-M., Collins, W., Fuglestvedt, J., Huang, J., Koch, D., Lamarque, J.-F., Lee, D., Mendoza, B., Nakajima, T., Robock, A., Stephens, G., Takemura, T., Zhang, H., 2013. Anthropogenic and natural radiative forcing. In: Stocker, T.F., Qin, D., Plattner, G.-K., Tignor, M., Allen, S.K., Boschung, J., Nauels, A., Xia, Y., Bex, V., Midgley, P.M. (Eds.), Climate Change 2013: The Physical Science Basis. Contribution of Working Group I to the Fifth Assessment Report of the Intergovernmental Panel On Climate Change. Cambridge University Press, pp. 659–740. https://doi.org/10.1017/CBO9781107415324.018.
Neubauer, S.C., 2021. Global warming potential is not an ecosystem property. Ecosystems 24 (8), 2079–2089. https://doi.org/10.1007/s10021-021-00631-x.
Neubauer, S.C., Megonigal, J.P., 2015. Moving beyond global warming potentials to quantify the climatic role of ecosystems. Ecosystems 18 (6), 1000–1013. https://doi.org/10.1007/s10021-015-9879-4.
Nilsson, M., Sagerfors, J., Buffam, I., Laudon, H., Eriksson, T., Grelle, A., Klemedtsson, L., Weslien, P., Lindroth, A., 2008. Contemporary carbon accumulation in a boreal oligotrophic minerogenic mire - A significant sink after accounting for all C-fluxes. Glob. Chang. Biol. 14 (10), 2317–2332. https://doi.org/10.1111/j.1365-2486.2008.01654.x.

Noyce, G.L., Varner, R.K., Bubier, J.L., Frolking, S., 2014. Effect of Carex rostrata on seasonal and interannual variability in peatland methane emissions. J. Geophys. Res.: Biogeosci. 119 (1), 24–34. https://doi.org/10.1002/2013JG002474.

Nugent, K.A., Strachan, I.B., Strack, M., Roulet, N.T., Rochefort, L., 2018. Multi-year net ecosystem carbon balance of a restored peatland reveals a return to carbon sink. Glob. Chang. Biol. 24 (12), 5751–5768. https://doi.org/10.1111/gcb.14449.

Nyberg, M., Black, T.A., Ketler, R., Lee, S.C., Johnson, M., Merkens, M., Nugent, K.A., Knox, S.H., 2022. Impacts of active versus passive re-wetting on the carbon balance of a previously drained bog. J. Geophys. Res.: Biogeosci. 127 (9), 1–19. https://doi.org/10.1029/2022JG006881.

Olson, D.M., Griffis, T.J., Noormets, A., Kolka, R., Chen, J., 2013. Interannual, seasonal, and retrospective analysis of the methane and carbon dioxide budgets of a temperate peatland. J. Geophys. Res.: Biogeosci. 118 (1), 226–238. https://doi.org/10.1002/jgrg.20031.

Otieno, D., Lindner, S., Muhr, J., Borken, W., 2012. Sensitivity of peatland herbaceous vegetation to vapor pressure deficit influences net ecosystem CO_2 exchange. Wetlands 32 (5), 895–905. https://doi.org/10.1007/s13157-012-0322-8.

Papale, D., Reichstein, M., Aubinet, M., Canfora, E., Bernhofer, C., Kutsch, W., Longdoz, B., Rambal, S., Valentini, R., Vesala, T., Yakir, D., 2006. Towards a standardized processing of Net Ecosystem Exchange measured with eddy covariance technique: algorithms and uncertainty estimation. Biogeosciences 3 (4), 571–583. https://doi.org/10.5194/bg-3-571-2006.

Park, H., Launiainen, S., Konstantinov, P.Y., Iijima, Y., Fedorov, A.N., 2018. Modeling the effect of moss cover on soil temperature and carbon fluxes at a tundra site in Northeastern Siberia. J. Geophys. Res.: Biogeosci. 123 (9), 3028–3044. https://doi.org/10.1029/2018JG004491.

Peichl, M., Öquist, M., Ottosson Löfvenius, M., Ilstedt, U., Sagerfors, J., Grelle, A., Lindroth, A., Nilsson, M.B., 2014. A 12-year record reveals pre-growing season temperature and water table level threshold effects on the net carbon dioxide exchange in a boreal fen. Environ. Res. Lett. 9 (5) https://doi.org/10.1088/1748-9326/9/5/055006.

Pugh, C.A., Reed, D.E., Desai, A.R., Sulman, B.N., 2018. Wetland flux controls: how does interacting water table levels and temperature influence carbon dioxide and methane fluxes in northern Wisconsin? Biogeochemistry 137 (1–2), 15–25. https://doi.org/10.1007/s10533-017-0414-x.

Reichstein, M., Subke, J.A., Angeli, A.C., Tenhunen, J.D., 2005. Does the temperature sensitivity of decomposition of soil organic matter depend upon water content, soil horizon, or incubation time? Glob. Chang. Biol. 11 (10), 1754–1767. https://doi.org/10.1111/j.1365-2486.2005.001010.x.

Rigg, B., Richardson, C.T., 1938. Profiles of Some Sphagnum Bogs of the Pacific Coast of North America Author (s): George B . Rigg and Carl T . Richardson Published by : ecological Society of America. Ecology 19 (3), 408–434.

Rinne, J., Tuittila, E.S., Peltola, O., Li, X., Raivonen, M., Alekseychik, P., Haapanala, S., Pihlatie, M., Aurela, M., Mammarella, I., Vesala, T., 2018. Temporal variation of ecosystem scale methane emission from a boreal fen in relation to temperature, water table position, and carbon dioxide fluxes. Glob. Biogeochem. Cycle. 32 (7), 1087–1106. https://doi.org/10.1029/2017GB005747.

Roulet, N.T., Lafleur, P.M., Richard, P.J.H., Moore, T.R., Humphreys, E.R., Bubier, J., 2007. Contemporary carbon balance and late Holocene carbon accumulation in a northern peatland. Glob. Chang. Biol. 13 (2), 397–411. https://doi.org/10.1111/j.1365-2486.2006.01292.x.

Ryu, Y., Baldocchi, D.D., Ma, S., Hehn, T., 2008. Interannual variability of evapotranspiration and energy exchange over an annual grassland in California. J. Geophys. Res. Atmos. 113, 1–16. https://doi.org/10.1029/2007JD009263.

Schaefer, K., Denning, A.S., Suits, N., Kaduk, J., Baker, I., Los, S., Prihodko, L., 2002. The effect of climate on interannual variability of terrestrial CO2 fluxes. Glob. Biogeochem. Cycle. 16 (4) https://doi.org/10.1029/2002GB001928.

Schaller, C., Hofer, B., Klemm, O., 2021. Greenhouse gas exchange of a NW German peatland, 18 years after rewetting. J. Geophys. Res.: Biogeosci. 127 (2) https://doi.org/10.1029/2020JG005960.

Shurpali, N.J., Verma, S.B., Kim, J., 1995. Carbon dioxide exchange in a peatland ecosystem. J. Geophys. Res. 100 (D7), 14319–14326.

Strachan, I.B., Pelletier, L., Bonneville, M.C., 2016. Inter-annual variability in water table depth controls net ecosystem carbon dioxide exchange in a boreal bog. Biogeochemistry 127 (1), 99–111. https://doi.org/10.1007/s10533-015-0170-8.

Strack, M., Price, J.S., 2009. Moisture controls on carbon dioxide dynamics of peat-Sphagnum monoliths. Ecohydrology 2, 34–41. https://doi.org/10.1002/eco.

Sulman, B.N., Desai, A.R., Saliendra, N.Z., Lafleur, P.M., Flanagan, L.B., Sonnentag, O., MacKay, D.S., Barr, A.G., Van Der Kamp, G, 2010. CO_2 fluxes at northern fens and bogs have opposite responses to inter-annual fluctuations in water table. Geophys. Res. Lett. 37 (19) https://doi.org/10.1029/2010GL044018.

Swenson, M., Regan, S., Bremmers, D., Lawless, J., Saunders, M., Gill, L., 2018. Carbon balance of a restored and cutover raised bog: comparison to global trends. Biogeosci. Discuss. 16, 713–731. https://doi.org/10.5194/bg-16-713-2019.

Teklemariam, T.A., Lafleur, P.M., Moore, T.R., Roulet, N.T., Humphreys, E.R., 2010. The direct and indirect effects of inter-annual meteorological variability on ecosystem carbon dioxide exchange at a temperate ombrotrophic bog. Agric. For. Meteorol. 150 (11), 1402–1411. https://doi.org/10.1016/j.agrformet.2010.07.002.

Thornley, J., Johnson, I., 1990. Plant and Crop Modelling: A Mathematical Approach to Plant and Crop Physiology. The Blackburn Press.

Ueyama, M., Iwata, H., Harazono, Y., 2014. Autumn warming reduces the CO_2 sink of a black spruce forest in interior Alaska based on a nine-year eddy covariance measurement. Glob. Chang. Biol. 20 (4), 1161–1173. https://doi.org/10.1111/gcb.12434.

Ueyama, M., Yazaki, T., Hirano, T., Futakuchi, Y., Okamura, M., 2020. Environmental controls on methane fluxes in a cool temperate bog. Agric. For. Meteorol. 281, 107852 https://doi.org/10.1016/j.agrformet.2019.107852. November 2019.

Vickers, D., Mahrt, L., 1997. Quality control and flux sampling problems for tower and aircraft data. J. Atmos. Oceanic Technol. 14, 512–526. https://doi.org/10.1175/1520-0426(1997)014<0512:QCAFSP>2.0.CO;2.

Wang, M., Wu, J., Lafleur, P.M., Luan, J., Chen, H., Zhu, X., 2018. Temporal shifts in controls over methane emissions from a boreal bog. Agric. For. Meteorol. 262 (March 2017), 120–134. https://doi.org/10.1016/j.agrformet.2018.07.002.

Wang, M., Wu, J., Luan, J., Lafleur, P., Chen, H., Zhu, X., 2017. Near-zero methane emission from an abandoned boreal peatland pasture based on eddy covariance measurements. PLoS One 12 (12), 1–21. https://doi.org/10.1371/journal.pone.0189692.

Webb, E.K., Pearman, G.I., Leuning, R., 1980. Correction of flux measurements for density effects due to heat and water vapour transfer. Q. J. R. Meteorolog. Soc. 106, 85–100.

Whalen, S.C., 2005. Biogeochemistry of methane exchange between natural wetlands and the atmosphere. Environ. Eng. Sci. 22 (1), 73–94. https://doi.org/10.1089/ees.2005.22.73.

Whitfield, P.H., Hebda, R.J., Jeglum, J.K., & Howie, S. (2006). Restoring the natural hidrology of Burns Bog, Delta, British Columbia – the key to the bog's ecological recovery. In A. Chantler (Ed.), *Water Under Pressure* (pp. 58–70). Proceedings of the CWRA Conference Vancouver.

Wilczak, J.M., Oncley, S.P., Stage, S.A., 2001. Sonic anemometer tilt correction algorithms. Bound. Lay. Meteorol. 99, 127–150. https://doi.org/10.1023/A:1018966204465.

Wilson, D., Farrell, C.A., Fallon, D., Moser, G., Müller, C., Renou-Wilson, F., 2016. Multiyear greenhouse gas balances at a rewetted temperate peatland. Glob. Chang. Biol. 22 (12), 4080–4095. https://doi.org/10.1111/gcb.13325.

Wutzler, T., Lucas-Moffat, A., Migliavacca, M., Knauer, J., Sickel, K., Šigut, L., Menzer, O., Reichstein, M., 2018. Basic and extensible post-processing of eddy covariance flux data with REddyProc. Biogeosciences 15 (16), 5015–5030. https://doi.org/10.5194/bg-15-5015-2018.

Yuan, W., Liu, S., Dong, W., Liang, S., Zhao, S., Chen, J., Xu, W., Li, X., Barr, A., Andrew Black, T., Yan, W., Goulden, M.L., Kulmala, L., Lindroth, A., Margolis, H.A., Matsuura, Y., Moors, E., Van Der Molen, M., Ohta, T., …, Vesala, T., 2014. Differentiating moss from higher plants is critical in studying the carbon cycle of the boreal biome. Nat. Commun. 5 https://doi.org/10.1038/ncomms5270.

Zhang, H., Tuittila, S., Korrensalo, A., Laine, A.M., Uljas, S., Welti, N., Kerttula, J., Maljanen, M., Elliott, D., Vesala, T., Lohila, A., 2021. Methane production and oxidation potentials along a fen—Bog gradient from southern boreal to subarctic peatlands in Finland. Glob. Chang. Biol. 27, 4449–4464. https://doi.org/10.1111/gcb.15740. April, 4449–4464.

Zieba, A., Ramza, P., 2011. Standard deviation of the mean of autocorrelated observations estimated with the use of the autocorrelation function estimated from the data. Metrol. Measur. Syst. XVIII (4), 529–542. https://doi.org/10.1017/cbo9780511921247.018.